Article:
Lu, T. orcid.org/0000-0002-6458-1217, Ren, J. orcid.org/0000-0001-9985-3430, Deng, X. et al. (1 more author) (2023) Numerical study of the autogenous shrinkage of cement pastes with supplementary cementitious materials based on solidification theory. Construction and Building Materials, 392. 131645. ISSN: 0950-0618

https://doi.org/10.1016/j.conbuildmat.2023.131645

Construction and Building Materials 392 (2023) 131645

Contents lists available at ScienceDirect

Construction and Building Materials

journal homepage: www.elsevier.com/locate/conbuildmat

Numerical study of the autogenous shrinkage of cement pastes with supplementary cementitious materials based on solidification theory

Tianshi Lu [a], Jie Ren [b], Xisheng Deng [a], Zhenming Li [c,*]

[a] School of Civil Engineering and Geomatics, Southwest Petroleum University, Chengdu, China
[b] Department of Civil and Environmental Engineering, University of Colorado Boulder, Boulder, CO, USA
[c] Department of Materials Science and Engineering, The University of Sheffield, Sheffield, United Kingdom

ARTICLE INFO

Keywords:
Autogenous shrinkage
Silica fume
Fly ash
Cement paste
Solidification theory

ABSTRACT

The addition of supplementary cementitious materials (SCMs), which is an effective method to reduce the CO_2 emission during the cement production, will change the autogenous shrinkage of early-age hydrating cementitious systems. In this paper the effect of different SCMs, i.e., silica fume and fly ash, on the physical properties and autogenous shrinkage of cement paste is studied, both experimentally and numerically. The experiment results show that autogenous shrinkages of cement pastes reduce significantly with the increase of water-binder ratio. The addition of fly ash will lead to smaller autogenous shrinkage while the influence of the dry densified silica fume on the autogenous shrinkage is not pronounced. A numerical simulation model, in which autogenous shrinkage is split up into an elastic part and a time-dependent part is proposed in this paper. The two parts are calculated separately. The simulation of the visco-elastic response of the cement paste to the internal driving force was performed by using a solidification theory model that takes the aging into consideration. The physical properties of different kinds of cement paste are experimentally investigated and the measured results are taken as input parameters of the simulation model. The simulated autogenous shrinkage of different kinds of cement pastes are compared with the measured results to verify the prediction of the proposed model.

1. Introduction

Global warming, which is primarily caused by the emission of greenhouse gases, is now a serious environmental problem. Carbon dioxide (CO_2) is a major component of greenhouse gases. According to Olivier [1], CO_2 contributes 73% to global total greenhouse gas emission during the period from 1970 to 2015. One of the principal sources of CO_2 emission is conventional ordinary Portland cement (OPC) production. During the production process of OPC clinker, a large amount of coal and petroleum coke is combusted. It was reported that 3.4% of global CO_2 emission was from fossil fuel combustion for cement production [2]. Therefore, reduction in CO_2 emission during the OPC clinker production process has a great significance on slowing global warming.

One of the effective ways to reduce the CO_2 emission of cement industry is the replacement of cement by supplementary cementitious materials (SCMs). SCMs are by-products of other industries with pozzolanic reactivity [3]. The commonly used SCMs include natural pozzolans, ground granulated blast furnace slag, fly ash and silica fume [3–7]. The utilization of SCMs can significantly reduce the dosage of OPC clinker and therefore decrease the CO_2 emission related to the OPC clinker production. Moreover, many researches show that the addition of SCMs can improve the performances of concrete, such as workability, durability and strength [4–11]. Due to their eco-friendly characteristics and ability to enhance the mechanical and durability properties of concrete, SCMs are now widely used in cementitious systems, e.g., in Ultra-High-performance concrete with low water-binder ratio [12–14].

After the mixing of cement and water, water is consumed and the internal relative humidity of the cementitious system decreases, which is known as self-desiccation [15]. The shrinkage of cement pastes and concretes related to self-desiccation is called autogenous shrinkage [16]. Traditionally, autogenous shrinkage is considered to be negligible when compared with other early age deformations of OPC concrete, e.g., drying shrinkage and chemical shrinkage. But due to its low water-cement ratio, the self-desiccation and corresponding autogenous shrinkage of Ultra-high-performance concrete are much greater than that of normal OPC concrete. Thus, the risk of early-age cracking induced by the restrained autogenous shrinkage has gained more and more attention [17–19].

* Corresponding author.
E-mail address: zhenming.li@sheffield.ac.uk (Z. Li).

https://doi.org/10.1016/j.conbuildmat.2023.131645
Received 15 March 2022; Received in revised form 4 April 2023; Accepted 1 May 2023
Available online 14 June 2023

Apart from water-binder ratio, the addition of SCMs in cementitious system also has a considerable impact on the autogenous shrinkage [20–23]. During the past few decades, many investigations about this topic have been carried out [23–25]. It was reported that the use of silica fume would increase the autogenous shrinkage [26–28], whereas the addition of fly ash in concrete resulted in smaller autogenous shrinkage [29–31]. However, most of the researches are only experimental studies without the deeper insight into the mechanisms of autogenous shrinkage. The variation of autogenous shrinkage of concrete with the addition of SCMs can be attributed to two factors, i.e., changes of the internal relative humidity of the pore system [32–34] and modification of physical properties of the binders, such as elastic modulus and compressive strength [4,21,35–39]. Both two factors are caused by the change of pore structure of cementitious system associated with the pozzolanic reaction of SCMs [40–43]. On the one hand, some cementitious materials with supplementary materials have a finer pore structure than that with pure OPC [44]. Finer pore structure leads to a smaller radius of water–air meniscus and larger internal driving force of autogenous shrinkage, e.g., capillary tension [45]. One the other hand, cementitious systems, e.g., OPC paste and concrete, are not ideally elastic materials. The deformation of cementitious systems includes two components, elastic deformation and time-dependent deformation, i.e., creep [16,19,35,46]. Both the elastic deformation and creep are determined by the physical properties of the material, namely elastic modulus and creep compliance. Numerous researches show that there is general agreement about the existence of a relationship between porosity and physical properties [47,48]. Therefore, the change of the microstructure of cementitious systems due to the addition of SCMs will affect the magnitude of the elastic deformation and creep and consequently the magnitude of autogenous shrinkage.

In order to predict the early-age deformation and evaluate the cracking potential of concrete with SCMs, a numerical simulation model about the time-dependent behaviour of cementitious systems is needed. Traditional analytical expressions and mathematical models about the time-dependent behaviour of cementitious systems [49–53] are not suitable for simulating the creep part of early-age autogenous shrinkage. One of the limitations is that most of the models, e.g., double and triple power law [50,51], are empirical and only proposed for the time-dependent deformation of certain kinds of cement paste or concrete. It is not suitable for some kinds of cement paste with SCMs. Another limitation is that the existing models are proposed to simulate the creep of hardened cement paste or concrete of which the microstructure and physical properties are almost invariable, e.g. after 28 days of curing [52,53]. In recent years, some new numerical models [54,55] about the basic creep of aging cementitious materials have been proposed. For early-age hydrating cementitious systems, the new proposed numerical models might be very useful for simulating the time-dependent behaviour.

About the prediction of autogenous shrinkage caused by self-desiccation, a lot of models have been proposed during the past few years. In 1978, a vast number of creep and shrinkage tests has been performed around the world and the database was gathered at Northwestern University [56]. This database was expanded to a RILEM database and used to develop RILEM Model B4. The RILEM Model B4 [57], as well as fib Model Code 2010 [58], was frequently used to predict the creep of concrete [59,60]. Recently, RILEM Model B4 was exploited to develop empirical predictive equations about the autogenous shrinkage [56] based on the test data. The equations are in form of power law of time. The effect of water-cement ratio, aggregate-binder ratio, cement type, supplementary materials and curing condition on the autogenous shrinkage were taken into consideration in these equations. Apart from RILEM Model B4 and fib Model Code 2010, there are also some proposed models [61–64] in which the autogenous shrinkage is taken as the visco-elastic-plastic response of the material to the internal driving force, e.g., capillary stresses.

In this paper, a numerical model of autogenous shrinkage of OPC paste with SCMs is proposed. The hydrating cement paste is considered as visco-elastic material in the proposed model and the elastic deformation and creep are calculated separately. The creep part of this model is based on the solidification theory [65,66] and takes the continuously changing physical properties of hardening cement paste into consideration. The effects of SCMs on the internal relative humidity of cement paste are also experimentally studied. Pure OPC paste (CEM I 42.5 N) and two kinds of cement paste with silica fume and fly ash are studied. The dosage of silica fume and fly ash is 10% and 30% by weight of the binder, respectively. Two water-binder ratios of these cement pastes, 0.3 and 0.4, are considered. The simulated autogenous shrinkages of different kinds of cement paste are compared with the measured results to evaluate the accuracy of the predictions.

2. Theoretical basis of this study

2.1. Driving force of autogenous shrinkage

Autogenous shrinkage is the volume reduction of sealed hydrating cementitious system under isothermal condition without any external load [33,63]. Although the mechanism of autogenous shrinkage is still under discussion, there is a consensus that autogenous shrinkage is related to the drop of internal relative humidity of the pore system [67–69]. Hydrating cementitious system is a partially saturated porous media and the status of the pore fluids in pore structure, including water and moist air, will change with the drop of internal relative humidity. According to Gray et al. and Gawin et al. [70,71], the changed pore fluids will exert pressure on the solid skeleton of cementitious system, which is the internal driving force of autogenous shrinkage and can be expressed:

$$\sigma^{tot} = [S\sigma^{wat} + (1 - S)\sigma^{gas}]\kappa \tag{1}$$

where σ^{tot} [MPa] is the total pressure exerted by the pore fluids on the solid skeleton; σ^{gas} [MPa] is the gas pressure; S [–] is the degree of saturation; κ [–] is the Biot coefficient; σ^{wat} [MPa] is the total pressure exerted by the water. According to Gawin et al. [71], the total pressure exerted by the water σ^{wat} is mainly made up by three parts:

$$\sigma^{wat} = \sigma^{cap} + \sigma^{dis} + \sigma^{sur} \tag{2}$$

where σ^{cap} [MPa] is capillary tension; σ^{dis} [MPa] is the disjoining pressure and σ^{sur} [MPa] is the surface tension of solid gel particles.

Among these different kinds of pressure exerted by the pore fluids, the gas pressure σ^{gas} is negligible compared with others [71]. In early-age sealed cement paste, the relative humidity is always above 75% [72], while the surface tension σ^{sur} only plays a significant role when relative humidity is lower than 50% [73]. Therefore, surface tension σ^{sur} can also be considered negligible for autogenous shrinkage. Some researchers proposed that the repulsive disjoining pressure σ^{dis} and attractive capillary tension σ^{cap} are related to each other and either capillary tension or disjoining pressure can be used to calculated autogenous shrinkage [19,74]. In this paper, the capillary tension σ^{cap} is employed to simulate the autogenous shrinkage of cement paste.

2.2. Numerical simulation model of autogenous shrinkage

The early age hardening cementitious systems, e.g., cement paste and concrete, exhibit visco-elastic characteristic. Once load is applied on the materials, a simultaneous volume change, which is called elastic deformation and governed by Hooke's law, occurs. Apart from elastic deformation, a time-dependent deformation which is named as creep can also be observed from the materials under sustained load. The flow in the cement paste, seepage, closing of internal voids and delayed elasticity are the most discussed mechanisms of creep [75,76]. During the past few decades, a lot of models about the deformation characteristic of cementitious materials have been proposed. Among these

models, solidification model proposed by Bazant [65,66] has been widely developed and used to predict the time-dependent behaviour of hardening and hardened cementitious materials [75,77,78]. In the solidification model, the total deformation of cementitious materials is made up of an elastic part, a viscoelastic part and a viscoplastic part (Equation (3). As shown in Fig. 1, the elastic part is represented as an elastic spring. The viscoelastic part is represented as a Kelvin-chain which includes an elastic spring and a dashpot. The viscoplastic part is considered as a dashpot and visualized in Fig. 1.

$$\varepsilon(t) = \varepsilon_e(t) + \varepsilon_c^{ve}(t) + \varepsilon_c^{vp}(t) \tag{3}$$

where $\varepsilon(t)$ [–] is the total deformation; $\varepsilon_e(t)$ [–] is the elastic part; $\varepsilon_c^{ve}(t)$ [–] is the viscoelastic part and $\varepsilon_c^{vp}(t)$ [–] is the viscoplastic part.

The elastic part of total deformation can be calculated according to Hooke's law which is expressed as:

$$\varepsilon_e(t) = \frac{\sigma(t)}{E(t)} \tag{4}$$

where $\sigma(t)$ [MPa] is the applied load at time t and $E(t)$ [MPa] is the elastic modulus of cement paste at time t.

In order to calculate the magnitude of creep, a lot of different formulae of creep compliance $J(t,t_0)$, which describes the relationship between the creep deformation and applied load, have been proposed by researchers [73,77–79]. Among these existing formulae, a closed-form one proposed by Hedegaard [75], which describes the time-dependent behaviour of concrete, is adopted and extended for the case of cement paste in this paper due to its concise expression. The creep compliance proposed by Hedegaard can be written as Equation (5). According to Hedegaard, the second and third term of Equation (5) together represent the viscoelastic part of creep. The fourth and fifth term of Equation (5) stand for the viscoplastic flow part of creep.

$$J(t,t_0) = \frac{1}{E_i} + \left(\frac{P_1}{K}\right)\left(\frac{1}{t_0-\beta}\right) ln\left[\frac{t_0}{t}\left(\frac{t-t_0}{\beta} + 1\right)\right] + P_1 ln\left(\frac{t-t_0}{\beta}+1\right) + \left(\frac{P_2}{Kt_0}\right)\left(\frac{t-t_0}{t}\right) + P_2 ln\frac{t}{t_0} \tag{5}$$

where $J(t,t_0)$ [MPa^{-1}] is the creep compliance; t_0 [days] is the time at loading; E_i [MPa] is the instantaneous modulus which is related to elastic modulus E [MPa], in this paper, it is taken as 1.43 E [75]; P_1 [MPa^{-1}] is the viscoelastic compliance constant depends on the compressive strength f_c [75], in this paper, it is expressed as $20.7e^{-0.06f_c}$. More details of the parameters E_i and P_1 can be found in literature [75,80,81]. P_2 [MPa^{-1}] is the flow constant and its value is taken as 7×10^{-6}; β [days] is the time constant whose value is 2×10^{-5} and K [days^{-1}] is the rate constant whose value is 0.5 [75].

If a hardened cementitious system is under a constant load σ [MPa], the creep deformation can be calculated with creep compliance as:

$$\begin{aligned}\varepsilon_c(t) &= J(t,t_0)\sigma \\ &= \left(\frac{1}{E_i} + \left(\frac{P_1}{K}\right)\left(\frac{1}{t_0-\beta}\right) ln\left[\frac{t_0}{t}\left(\frac{t-t_0}{\beta}+1\right)\right] + P_1 ln\left(\frac{t-t_0}{\beta}+1\right) \\ &\quad + \left(\frac{P_2}{Kt_0}\right)\left(\frac{t-t_0}{t}\right) + P_2 ln\frac{t}{t_0}\right)\sigma\end{aligned} \tag{6}$$

For early-age cement paste, the skeleton gets stronger with hydration process as shown in Fig. 2. The physical properties of cement paste related to the microstructure, e.g., elastic modulus and compressive strength, changes with the evolution of the solid skeleton of cement paste. Meanwhile, the internal relative humidity decreases and corresponding capillary tension increases. The capillary tension is the one of the main mechanisms of autogenous shrinkage. In order to predict the creep part of early-age autogenous shrinkage, the increasing driving force and changing physical properties of cement paste should be taken into consideration in the solidification model.

According to Hedegaard [66], at the a given time t_n (as shown in Fig. 2) the creep compliance rate can be express as:

$$\dot{J}(t_n,t_0) = \left(\frac{1}{Kt_n}+1\right)\left(\frac{P_1(t_n)}{t_n-t_0+\beta} + \frac{P_2}{t_n}\right) \tag{7}$$

The increment of creep $\Delta\varepsilon_c(t_n)$ (Fig. 2) that formed from time t_n to time $t_n+\Delta t$ under the internal driving force $\sigma(t_n)$ can be calculated as:

$$\Delta\varepsilon_c(t_n) = \sigma(t_n)\dot{J}(t_n,t_0)\Delta t = \sigma(t_n)\left(\frac{1}{Kt_n}+1\right)\left(\frac{P_1(t_n)}{t_n-t_0+\beta} + \frac{P_2}{t_n}\right)\Delta t \tag{8}$$

The time-dependent part of autogenous shrinkage $\varepsilon_c(t_{n+1})$ is the summation of increments of creep that formed before time t_{n+1} and it can be expressed as:

$$\begin{aligned}\varepsilon_c(t_{n+1}) &= \Delta\varepsilon_c(t_n) + \varepsilon_c(t_n) \\ &= \sigma(t_n)\left(\frac{1}{Kt_n}+1\right)\left(\frac{P_1(t_n)}{t_n-t_0+\beta} + \frac{P_2}{t_n}\right)\Delta t + \sum_{i=1}^{n}\Delta\varepsilon_c(t_i)\end{aligned} \tag{9}$$

For the tri-axial internal load condition, which is the case for autogenous shrinkage, combining Eq. (1) and Eq. (9), the creep part of autogenous shrinkage can be calculated as:

$$\varepsilon_c(t_{n+1}) = S\sigma^{cap}(t_{n+1})\kappa(1-2\vartheta)\left(\frac{1}{Kt_n}+1\right)\left(\frac{P_1(t_n)}{t_n-t_0+\beta} + \frac{P_2}{t_n}\right)\Delta t + \sum_{i=1}^{n}\Delta\varepsilon_c(t_i) \tag{10}$$

For the elastic part of autogenous shrinkage, the Coussy's method [82] which takes the contribution of the interface energy into account, should be introduced to replace the average capillary pressure in Eq. (1)

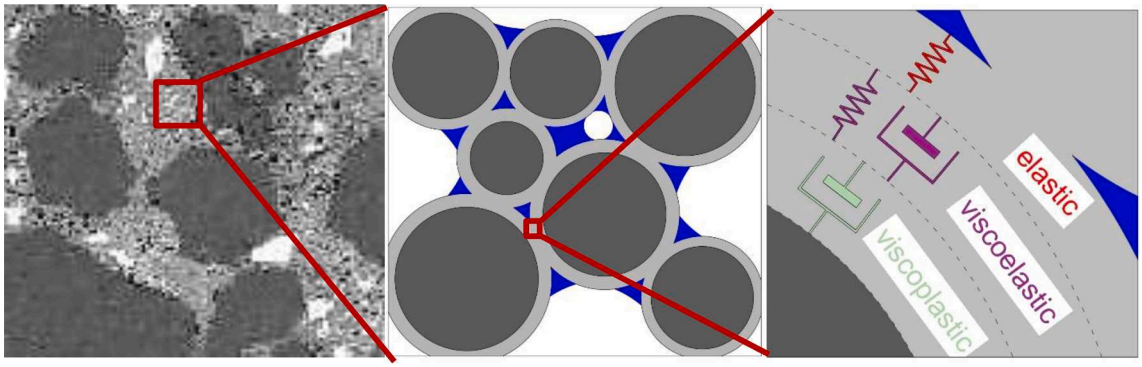

Fig. 1. Multi-scale structure of concrete: (a) concrete; (b) schematic microstructure of cement paste; (c) schematic microstructure of different layers of cement paste (after Bazant [64] and Abate [69]).

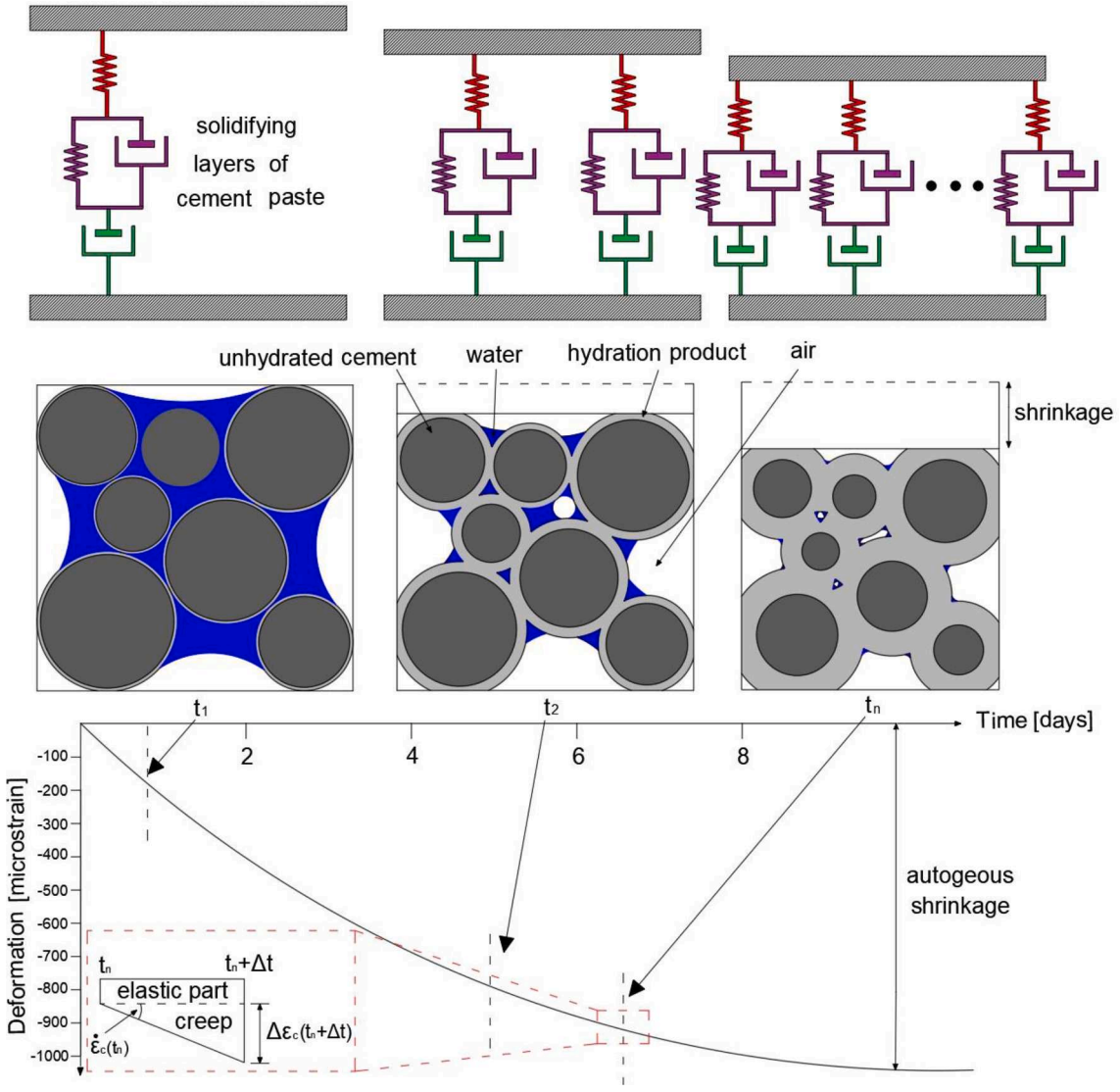

Fig. 2. Schematic representation of evolving solidifying layers, microstructure and autogenous shrinkage of hardening cement paste.

by the equivalent pore pressure as:

$$\varepsilon_e(t_{n+1}) = \frac{(S\sigma^{cap}(t_{n+1}) + U)\kappa}{E(t_{n+1})}(1-2\vartheta) = \frac{(S\sigma^{cap}(t_{n+1}) + \int_S^1 \sigma^{cap}(S)dS)\kappa}{E(t_{n+1})}(1-2\vartheta) \quad (11)$$

where ϑ [–] is the Poisson's ratio and U [Pa] is the interface energy. According to Hu [83], interface energy is relatively low at high saturation degrees in the self-desiccation case, therefore the elastic part of autogenous shrinkage is calculated in a simplified form in this paper as:

$$\varepsilon_e(t_{n+1}) = \frac{S\sigma^{cap}(t_{n+1})\kappa}{E(t_{n+1})}(1-2\vartheta) \quad (12)$$

The total autogenous shrinkage can be calculated as the summation of the elastic part and creep:

$$\varepsilon(t_{n+1}) = \varepsilon_e(t_{n+1}) + \varepsilon_c(t_{n+1}) \quad (13)$$

2.3. Calculation of autogenous shrinkage

In the proposed model, the autogenous shrinkage of hardening cement paste is the sum of the elastic and the creep part which can be calculated with Equation (12) and Equation (10) respectively. The calculation equations of elastic modulus, degree of saturation and capillary tension is given in Section 5.1-5.3. The flow chart of the whole calculation procedure is shown in Fig. 3.

3. Materials and experiments

The materials used in this study are OPC (CEM I 42.5 N), silica fume and fly ash. OPC (CEM I 42.5 N) is made up of four main mineral compounds: C_3S 67.1%, C_2S 5.9%, C_3A 7.8% and C_4AF 9.6%. The particle size distributions of these materials which were measured by laser diffraction are presented in Fig. 4. The mean particle sizes of Portland cement, silica fume and fly ash are 22 μm, 23 μm and 18 μm. From Fig. 4 it can be noticed that the mean particle size of silica fume is not significantly smaller than that of Portland cement. This is due to the fact that the silica fume used in study is dry densified silica fume. According to Diamond [84], the particle size of dry densified silica fume is close to that of OPC. More information about dry densified silica fume can also be found in Diamond's paper [84]. The chemical compositions of these materials are given in Table 1.

Six different kinds of cement paste mixtures are studied in this paper. Pure Portland cement pastes (CEM I 42.5 N) are prepared as reference. Silica fume cement pastes are made of Portland cement (CEM I 42.5 N)

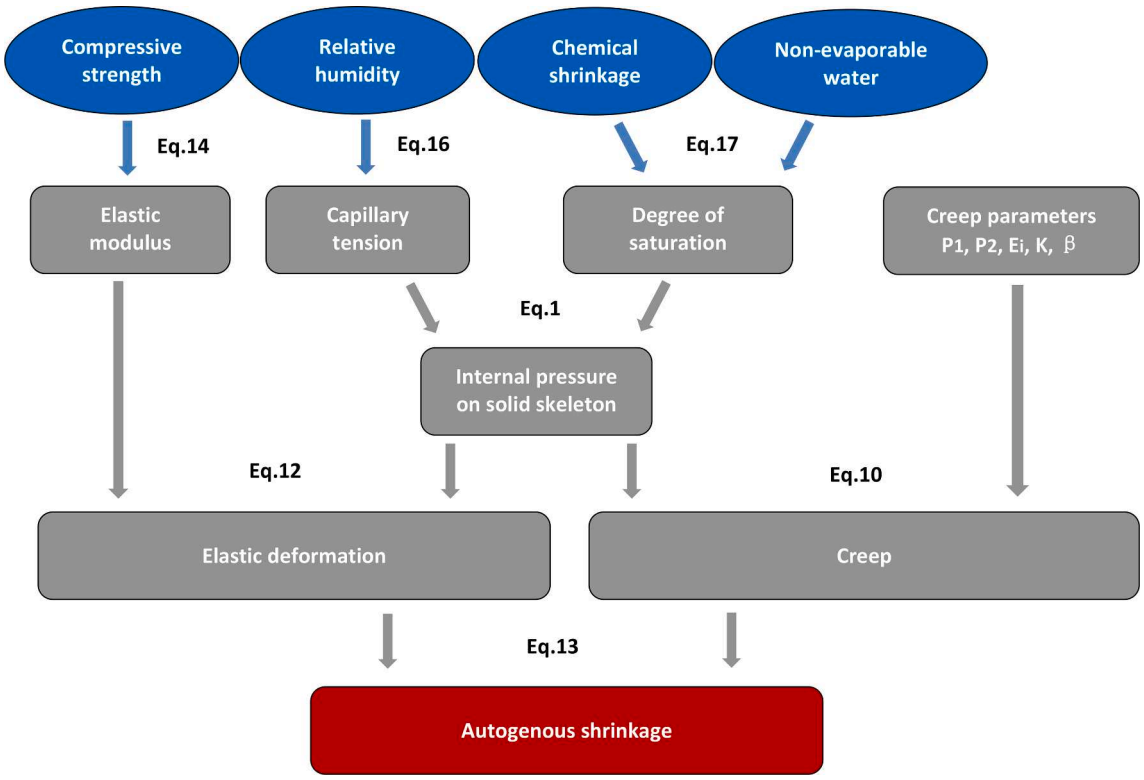

Fig. 3. Flow chart of the proposed model of autogenous shrinkage.

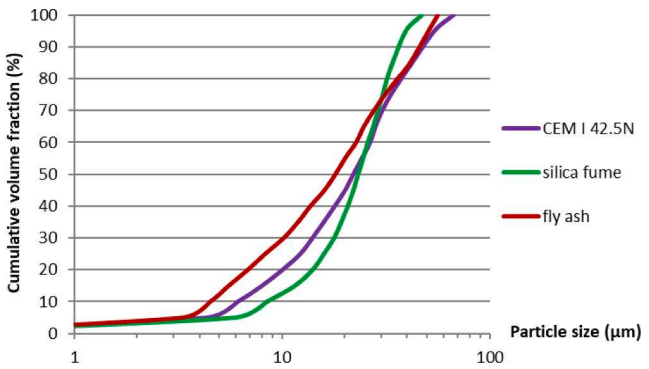

Fig. 4. Particle size distribution of materials used in this study.

Table 1
Chemical composition of the materials used in this study.

Chemical composition (% by weight)	CEM I 42.5 N	Silica fume	Fly ash
CaO	64.4	0.39	7.14
SiO_2	20.36	97.2	48.4
Al_2O_3	4.96	0.51	31.4
Fe_2O_3	3.17	0.18	4.44
SO_3	2.57	0.26	1.18
Na_2O	0.14	–	0.72
K_2O	0.64	1.04	1.64
MgO	2.09	–	1.35
Total	98.33	99.58	96.7

and dry densified silica fume. Fly ash cement pastes are made of Portland cement (CEM I 42.5 N) and fly ash powder. The dosage of silica fume and fly ash is 10% and 30% by weight of the binder, respectively. The water/binder ratios are 0.3 and 0.4. Cementitious material is mixed with water in a 5L epicyclic Hobart mixer. The mixing procedure is according to ASTM 305–99 [85]. The mixture composition of different kinds of cement pastes is listed in Table 2.

3.1. Final setting time

The final setting time of sealed specimens was determined with a Vicat apparatus (penetration method) according to the procedure described in standard EN 196–3 [86]. The diameters of the upper surface and the bottom surface of the sample were 70±1 mm and 80±1 mm, respectively. The height of the sample was 40±0.2 mm. The sample was cured in sealed condition at 20 °C before the test.

3.2. Internal relative humidity

The internal relative humidity of cement paste was measured by Rotronic hygroscopic DT stations equipped with HC2-AW RH station probes (Fig. 5a) with an accuracy ±0.5%. Two samples were tested for each mixture. The diameter of the sample was 30 mm and the thickness of the sample was less than 7 mm. During the measurement, the sample was placed in a sample holder which was immersed in the water bath at 20±0.1 °C (Fig. 5b). The humidity probe was placed above the sample. The humidity probes were calibrated by three saturated salt solutions with known constant relative humidity in the range of 65–95% before and after each test. The internal relative humidity of the specimen was continuously measured every 3 min for 7 days after mixing.

Table 2
Mixture composition of different kinds of cement pastes used in this study (% by weight).

Name	Water-binder ratio	CEM I 42.5 N	Silica fume	Fly ash
OPC 0.3	0.3	100	0	0
SF 0.3	0.3	90	10	0
FA 0.3	0.3	70	0	30
OPC 0.4	0.4	100	0	0
SF 0.4	0.4	90	10	0
FA 0.4	0.4	70	0	30

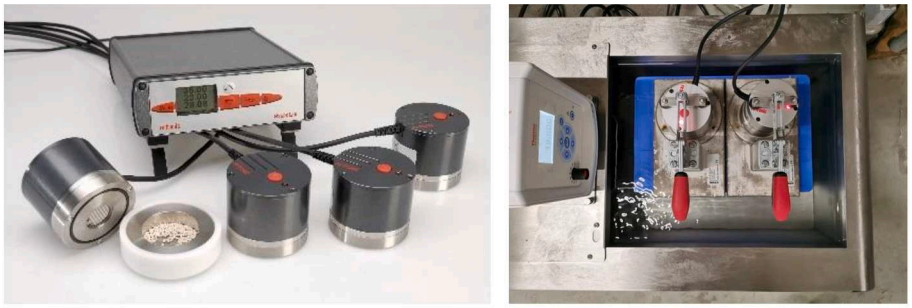

(a) Equipment for internal relative humidity measurement (b) Top view of temperature-controlled water bath

Fig. 5. Measurement of internal relative humidity.

3.3. Chemical shrinkage

In order to measure the chemical shrinkage, 50 g cement paste was cast in an Erlenmeyer flask. The capacity of the flask was 250 ml. The thickness of the sample was 8 mm. The flask was fully filled with paraffin oil. There was a thin layer of water between the sample and paraffin oil. The water level of a graduated tube, which was fixed on the rubber stopper of the flask, was recorded to calculate the chemical shrinkage. The flask was immersed in a water bath whose temperature is kept at 20 °C. Measurements lasted for 7 days. The chemical shrinkage is the ratio between the absolute volume reduction of cement paste and the mass of the binder [87]. Two specimens were tested simultaneously for each mixture.

3.4. Non-evaporable water content

For determining the non-evaporable water content, about 10 g of fresh cement paste was cast and cured in a sealed plastic vial at 20 °C. The samples were ground to powder and immersed in liquid nitrogen to stop hydration at the required ages, i.e. 1 day, 3 day and 7 day. The powder was divided into two approximately equal parts which were kept in an oven at 105 °C for 20 h. After removing from the oven, the samples were weighed and placed in a furnace at 950 °C for 4 h. When the samples were taken out from the furnace their mass was measured again. The average difference of the mass measurements between 105 °C and 950 °C was calculated as the non-evaporable water content.

3.5. Compressive strength

The size of cubic specimen of compressive strength test was 40 × 40 × 40 mm^3. The compressive strength at age of 1, 3 and 7 days were measured. Before the test the cubes were cured in sealed condition at 20 °C. For each measurement three samples were tested.

3.6. Autogenous shrinkage

The autogenous deformation of mixtures was measured according to ASTM C1698-09 [88] standard developed by Jensen and Hansen [89]. Freshly mixed cement paste was cast under vibration into a corrugated tube and the tube was sealed by plugs and sealing glue (Fig. 6). The length of the tube was approximately 430 mm and the outer diameter was 29 mm. The autogenous shrinkage of specimens was recorded every 5 min by linear variable differential transformers (LVDTs). Specimens and test instruments were immersed in a box filled with glycol, of which the temperature was kept at 20±0.1 °C. Three parallel samples were measured for each mixture with a measurement accuracy of ±5 μm/m.

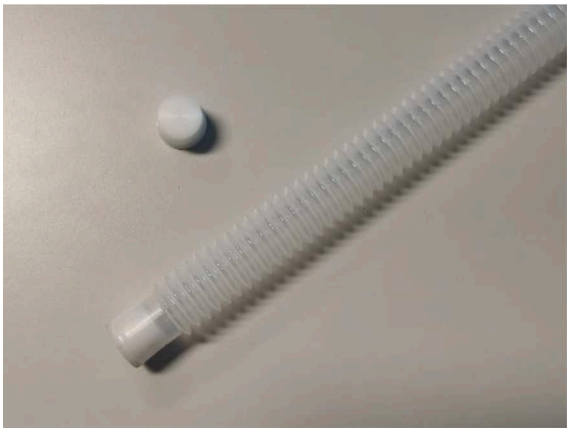

Fig. 6. Corrugated tube for autogenous shrinkage measurement.

4. Experimental results and discussion

4.1. Final setting time

The measured results of final setting time of different kinds of cement paste are shown in Fig. 7. From Fig. 7 it can be noticed that the measured final setting time of all kinds of cement paste prolongs with the increase of water binder ratio. This result is in line with the finding of Marar [90] and Hu [91]. The longer final setting time of cement pastes with higher water-binder ratio can be attributed to effect of w/b ratio on the distance among cement particles. The final setting time is the time when the paste completely loses its plasticity and has certain strength to resist pressure. After mixing hydration reaction takes place in cement paste and hydration product forms around the cement particles. The expansive cement particles become interconnected and a solid skeleton which is the key of strength is formed. The contact area between the interconnected cement particles is the most important parameter of the strength of the cement paste [47]. For cement paste with higher water-binder ratio the interparticle distance is larger so that more time is needed for the hydrating system to form sufficient contact area and strong enough solid skeleton to resist pressure. Therefore, the final setting time increases with water-binder ratio of all different kinds of cement pastes.

Fig. 7 also shows that the addition of fly ash will significantly increase the final setting time compared with that of other two kinds of cement paste with same water-binder ratio. Similar result was also reported by Dave [92]. According to Taylor [3], the early age reaction activity of fly ash is lower than that of Portland cement. The 30-percentage replacement of low active fly ash leads to higher effective water-binder ratio. The higher water binder ratio results in longer final setting time as discussed in last paragraph.

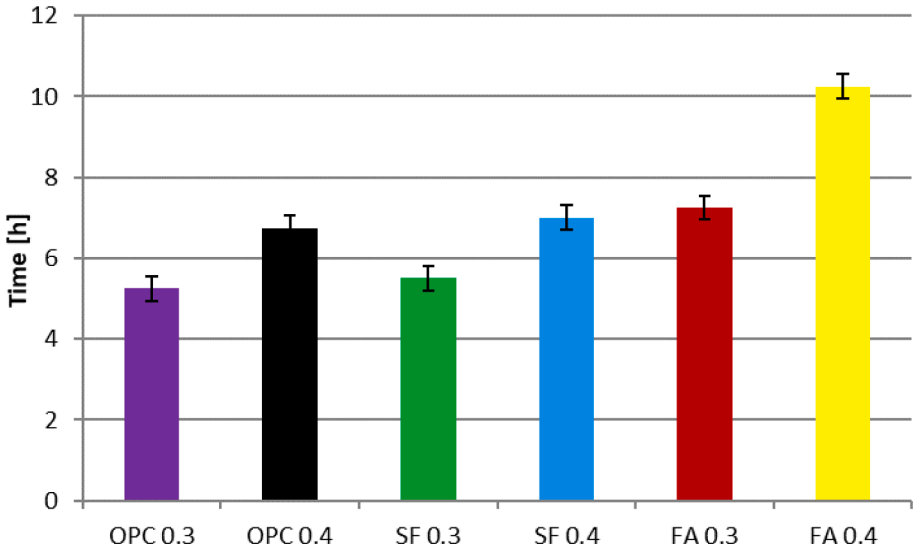

Fig. 7. Measured final setting time of different kinds of cement paste.

4.2. Internal relative humidity

In Fig. 8 the measured internal relative humidity of cement pastes with water-binder ratio of 0.3 and 0.4 as a function of age is presented. After the start of measurement, some time is needed for the moisture equilibrium between the sensor and sample to be reached. During this period, the number of the sensor increases with time. When the moisture equilibrium is reached, the measured value of the sensor is the real internal relative humidity which decreases with time.

Fig. 8 shows that the relative humidity of silica fume cement paste is higher than that of Portland cement paste with same water-binder ratio. From Fig. 4 it can be found that the particle size distribution of silica fume is close to that of Portland cement. According to Diamond [84], dry densified silica fume is primarily in the form of linked clusters of particles. The early-age reaction activity of dry densified silica fume is lower than that of Portland cement paste. More free water exists in the pore structure of silica fume cement paste which leads to higher internal relative humidity. The lower early-age reaction activity of dry densified silica fume is also confirmed by the experimental results of non-evaporable water content and compressive strength.

Fig. 8 also shows that the drop of internal relative humidity of fly ash cement paste is much smaller than that of Portland cement paste with same water-binder ratio during the first seven days. Similar results were also reported by Varga [34]. The reason of the smaller drop of internal relative humidity of fly ash cement paste is same to that of silica fume cement paste, i.e., low reaction activity of fly ash at the early age.

4.3. Chemical shrinkage

Chemical shrinkage will be used for calculating degree of saturation of cement paste. The measured chemical shrinkages of Portland cement, silica fume cement and fly ash cement are shown in Fig. 9. From Fig. 9 it can be noticed that the chemical shrinkage of the fly ash cement paste is much smaller than that of other two kinds of cement paste. This result is in accordance with the finding of Varga [34]. It is generally accepted that there is a relationship between chemical shrinkage and the degree of hydration [93,94]. The amount of inactive minerals in fly ash, e.g., mullite and quartz, is larger than that of Portland cement and silica fume [3]. Fly ash cement hydrates slower at early age which leads to smaller chemical shrinkage [95].

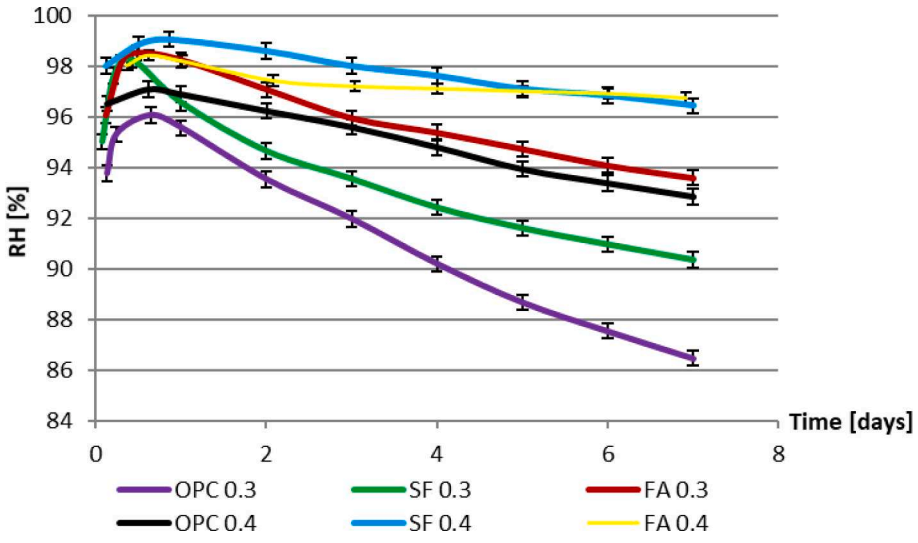

Fig. 8. Measured internal relative humidity of different kinds of cement paste.

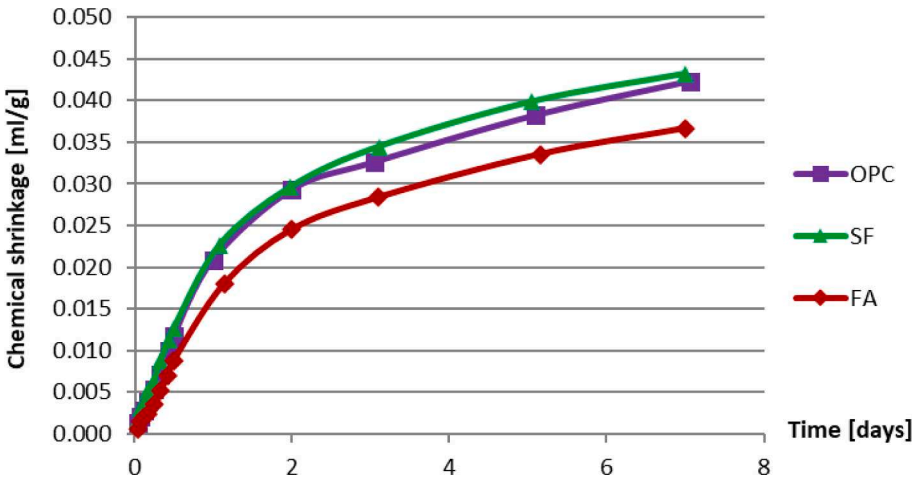

Fig. 9. Measured chemical shrinkage of different kinds of cementitious binders.

4.4. Non-evaporable water content

In Fig. 10 the measured non-evaporable water contents of cement pastes with water-binder ratio of 0.3 and 0.4 are shown. It can be noticed that the measured non-evaporable water contents of silica fume cement paste are lower than that of Portland cement paste with same water-binder ratio. This finding is in accordance with the results reported by Yogendran [96] and Zhang [97]. The low water binding capacity of silica fume during the hydration is an important reason for this phenomenon [3]. The low water binding capacity of silica fume leads to less chemical bound water. Another reason of the low measured non-evaporable water contents of silica fume is the low early-age reaction activity of dry densified silica fume. Lower reaction activity results in lower degree of hydration and less water consumption during the early-age hydration. Fig. 10 also shows that the non-evaporable water content in fly ash cement pastes is lower than that in ordinary Portland cement pastes with the same water-binder ratio at the same curing age. Similar measurement results are also reported by Maltais [98] and Schwarz [99]. The reason of this phenomenon is similar to that of silica fume containing cement paste.

4.5. Compressive strength

The measured compressive strengths of the all mixtures are provided in Fig. 11. For all kinds of cement paste, the compressive strength decreases with the increase of water-binder ratio. A lot of researchers have reported similar measurement results [100–102]. According to Singh [102], the microporosity of the cement paste is a function of the water-binder ratio. The higher water-binder ratio, the higher porosity and looser skeleton structure of cement paste which result in lower strength.

From Fig. 11 it can be found that the addition of silica fume will have negative effect on the compressive strengths of cement pastes. This is contrary to common sense that the use of silica fume will enhance the strength of concrete. Toutanji [103] pointed out the enhancement of compressive strength of concrete with silica fume is caused by the improvement of the interfacial transition zone (ITZ) between cement paste and aggregate. For the silica fume cement pastes without sand and aggregate, there is no strengthening effect. Fig. 11 also shows that the compressive strength of fly ash cement paste is lower than that of Portland cement paste with same water-binder ratio. Ramezanianpour [38] attributed this to the higher total and capillary porosity of fly ash cement paste.

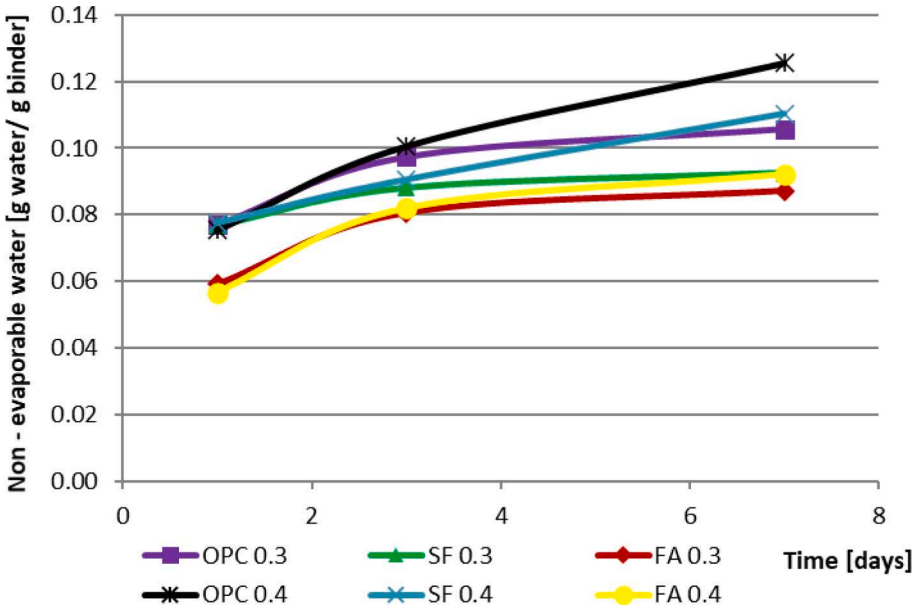

Fig. 10. Measured non-evaporable water content of different kinds of cement paste.

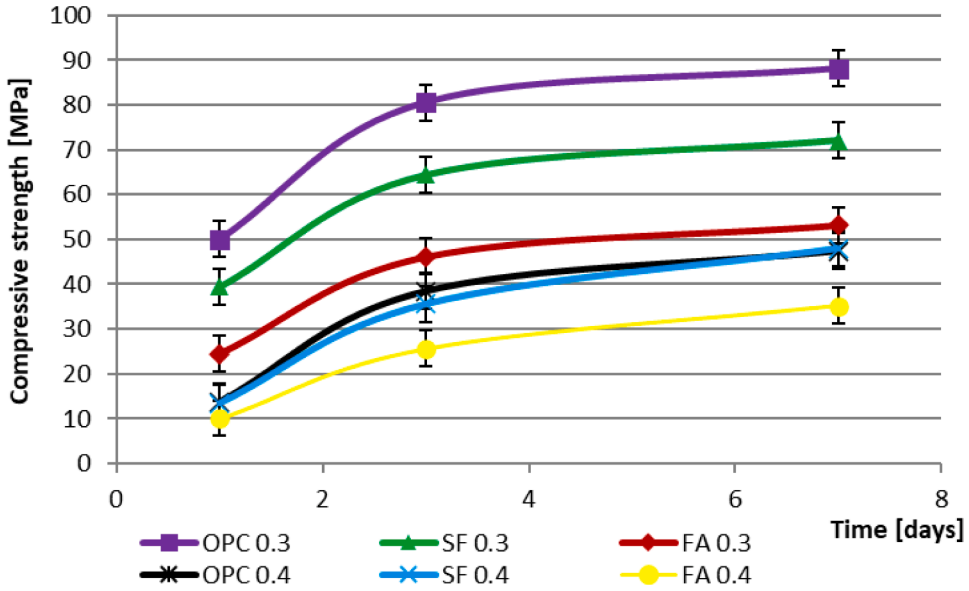

Fig. 11. Measured compressive strength of different kinds of cement paste.

4.6. Autogenous shrinkage

The development of autogenous deformations of different kinds of cement paste with time is shown in Fig. 12. The final setting time is the starting point of measurement. From Fig. 12 a fast shrinkage can be noticed after final setting. After a short period of swelling the specimens shrink steadily. According to some researchers [104–107] taking the final setting time as the starting point of autogenous shrinkage is questionable. The start of autogenous shrinkage is defined as the time when the cementitious materials develop sufficient structure to enable tensile stress transfer through the concrete [108,109]. It is not necessarily identical with the final setting time [110]. Bjøntegaard [111] proposed that the time when the maximum swelling is reached can be taken as the beginning of the autogenous shrinkage and this approach is adopted in this paper. But it should be noticed that the early-age deformations observed on macroscale are the result of expansion and shrinkage processes which develop simultaneously. When shrinkage is dominant, the external volume of cement paste will decrease. But the mechanisms of expansion still exist and play a role in the early-age autogenous deformation. The ignorance of any influence of expansion mechanism in the simulation model might lead to an overestimated autogenous shrinkage.

The autogenous shrinkage of different kinds of cement pastes after the maximum swelling is shown in Fig. 13. From Fig. 13 it can be observed that there is a significant effect of the addition of SCMs on autogenous shrinkage. The effect of the addition of SCMs on autogenous shrinkage will be detailed discussed in the following section.

4.7. Discussion

From the results of measurements, it can be noticed that the starting time of different measurements is not the same. For example, some time is needed for the moisture equilibrium between the sensor and sample to be reached in the relative humidity test. There are two kinds of starting time of autogenous shrinkage, i.e., final setting time and after the maximum swelling. In order to avoid unnecessary misunderstanding, the starting time of different measurements of all mixtures is given in Table 3. In the next section of simulation results, all the calculations start

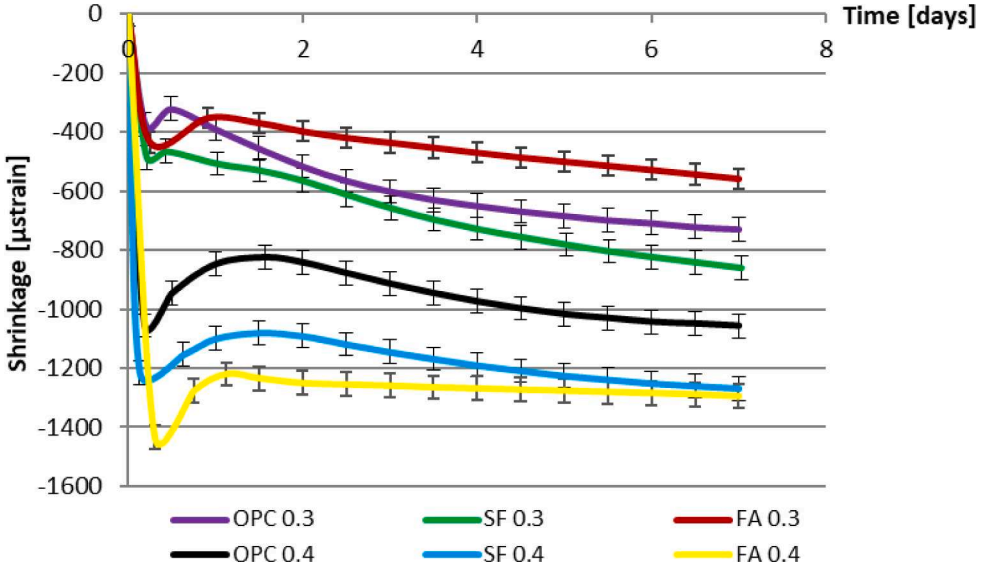

Fig. 12. Measured autogenous shrinkage of different kinds of cement paste (Starting time: final setting time).

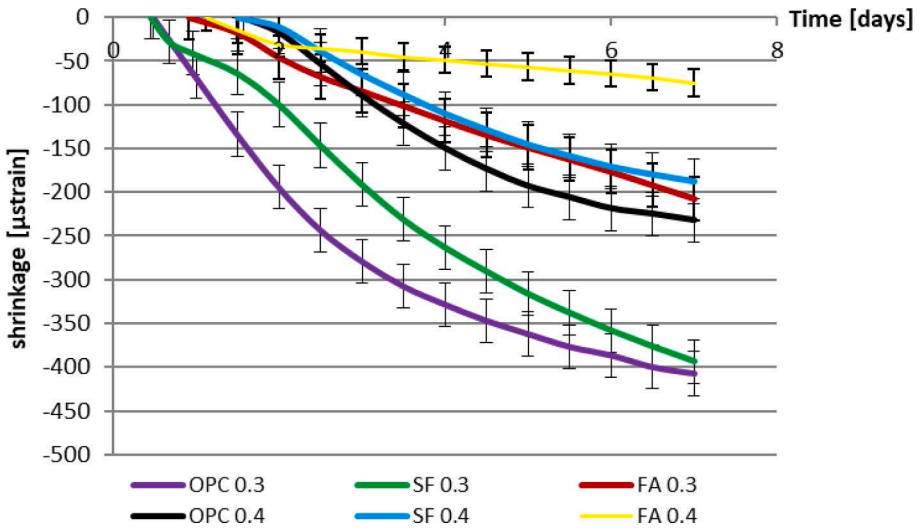

Fig. 13. Measured autogenous shrinkage of different kinds of cement paste (Starting time: after the maximum swelling).

Table 3
Starting time of different measurements in this study (The time 0 is when the cement is mixed with water).

Measurement	OPC 0.3 (days)	OPC 0.4 (days)	SF 0.3 (days)	SF 0.4 (days)	FA 0.3 (days)	FA 0.4 (days)
Internal relative humidity	0.24	0.33	0.23	0.55	0.28	0.36
Chemical shrinkage	0	0	0	0	0	0
Autogenous shrinkage	0.22	0.28	0.23	0.29	0.30	0.43
Autogenous shrinkage – After maximum swelling	0.71	1.70	0.68	1.94	1.60	1.58

at the time when the cement is mixed with water. The calculated autogenous shrinkage is plotted after the final setting time to be identical with the measured results.

5. Simulation results of material parameters and autogenous shrinkage

In order to simulate the autogenous shrinkage of cement pastes by using the proposed numerical model, elastic modulus E, capillary tension σ^{cap} and degree of saturation S should be determined (Eq. (10) and Eq. (12)) first.

5.1. Elastic modulus

In the proposed numerical model of autogenous shrinkage, the elastic modulus E [MPa] is needed for calculation of elastic deformation (Eq. (12)). Previous researches showed that elastic modulus and compressive strength of cementitious material are related and a lot of calculating equations of elastic modulus have been proposed [112,113]. In this paper, the equation developed by Takafumi (Eq. (14)) [113] is used to calculate the elastic modulus. The calculated elastic modulus of different kinds of cement paste based on the measured compressive strength (Fig. 14(a)) are presented in Fig. 14(b).

$$E = k_1 k_2 \varphi f_c^{1/3} \rho^2 \tag{14}$$

where f_c [MPa] is the compressive strength; ρ [Kg/m^3] is the density; φ [–] is a fitting coefficient; k_1 [–] and k_2 [–] are the correction factor related to the aggregate and SCMs. For cement paste,k_1 is taken as 1 because there is no effect of aggregate on the elastic modulus of cement paste. k_2 is related to the type of supplementary material and its value of different binders is given in Table 4. φ is a fitting coefficient, its value is taken as 0.0015 [113].

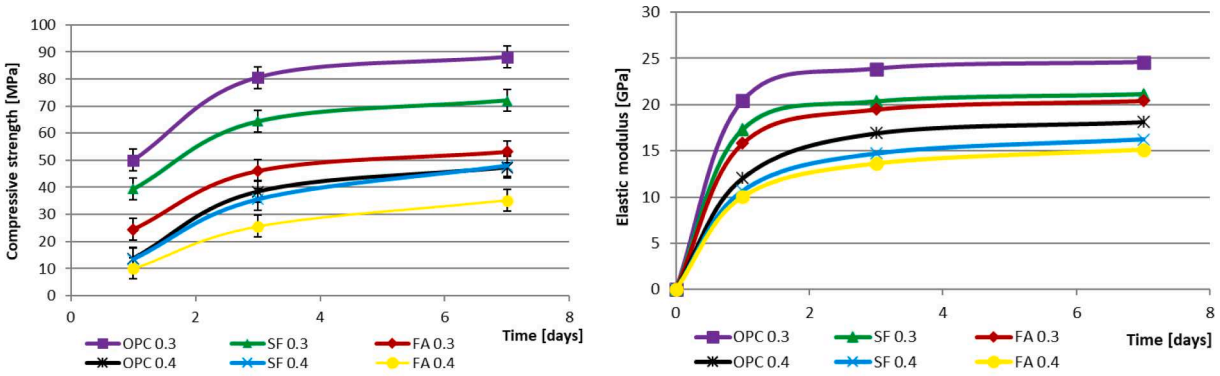

(a) Measured compressive strength (b) Elastic modulus calculated with Eq. 14

Fig. 14. Measured compressive strength and calculated elastic modulus of different kinds of cement paste.

Table 4
Practical values of correction factor k_2 for pastes made with different binders [113].

Type of addition	k_2
Silica fume, ground-granulated blast-furnace slag, fly ash	0.95
Fly ash	1.1
Addition other than above	1.0

5.2. Capillary tension

As discussed in Section 2.1, capillary tension σ^{cap} [MPa] is considered as the major component of internal driving force of autogenous shrinkage in this paper. The capillary tension in the pore fluid is related to the water-air menisci in the partly empty pores. Capillary tension puts the solid skeleton in compression, which goes along with a decrease of the volume of the cement paste. The magnitude of capillary tension is determined by the radius of water-air menisci, which is also named Kelvin radius γ_k [μm]. The Kelvin radius is a function of internal relative humidity (Eq. (15)) [114]. With the drop of internal relative humidity, caused by self-desiccation of hydrating cement paste, the Kelvin radius decreases and capillary tension increases which result in increasing autogenous shrinkage.

$$r_k = -\frac{2\gamma V_W}{lnRH_K RT} = -\frac{2\gamma V_W}{ln\frac{RH}{RH_S} RT} \tag{15}$$

where γ [N/m] is the surface tension of the pore solution; RH_K [–] is the internal relative humidity related to air-water menisci; RH [–] is the measured relative humidity; RH_S the effect of dissolved ions on relative humidity, in this paper, its value is taken as 0.97 [35,115]; V_m [m^3/mol] is the molar volume of the pore solution is taken as the value of molar volume of water, i.e., 18.02×10^{-6} m^3/mol in this study [116]; R [J/(mol•K)] is the universal gas constant and T [K] is the absolute temperature.

According to Laplace law [45,114], the calculation equation of capillary tension is:

$$\sigma_{cap} = \frac{RTlnRH_K}{V_W} = \frac{RTln\frac{RH}{RH_S}}{V_W} \tag{16}$$

The calculated capillary tension of different kinds of cement paste based on the measured relative humidity (as shown in Fig. 15(a)) is shown in Fig. 15(b). The beginning of the calculation is the peak of the measured relative humidity when the moisture equilibrium between the sensor and sample is reached.

5.3. Degree of saturation

In order to calculate the autogenous shrinkage caused by the internal pressure exerted by pore fluids, i.e., capillary tension, the degree of saturation S [–] should be determined (Eqs. (10) and (12)). According to Powers [117], the degree of saturation can be calculated as:

$$S_w = \frac{V_{ew}}{V_p} = \frac{V_{iw} - V_{new}}{V_{iw} - V_{new} + V_{cs}} \tag{17}$$

where V_{ew} [m^3/m^3] is unit evaporable water content; V_p [m^3/m^3] is the unit pore volume; V_{iw} [m^3/m^3] is the unit initial water content; V_{cs} [m^3/m^3] is the unit volume of chemical shrinkage and V_{new} is the unit non-evaporable water content.

In this paper, the degree of saturation of different kinds of cement paste is calculated with Eq. (17) based on the measured evaporable water content (Fig. 16(a)). The calculated results are shown in Fig. 16 (c).

5.4. Autogenous shrinkage

Based on the calculated early-age parameters of cement paste, i.e., elastic modulus, capillary tension and degree of saturation, the autogenous shrinkage of different kinds of cement paste can be simulated by using the proposed model. As discussed in Section 4.6, the measured deformation after the maximum swelling is taken as the autogenous shrinkage and used to verify the prediction of the proposed simulation models.

5.4.1. OPC paste with water-binder ratio of 0.3 and 0.4

Fig. 17(a and b) show the measured and calculated autogenous shrinkage of Portland cement pastes with water-binder ratio 0.3 and 0.4 respectively. The measured autogenous shrinkage of cement paste after maximum swelling is used to validate the simulation results. The contributions of elastic deformation and creep to autogenous shrinkage are presented in these figures. From Fig. 17(a and b) it can be noticed that creep plays an important role in autogenous shrinkage and the autogenous shrinkage of OPC paste can be better predicted by taking the creep into consideration. Similar report can be found in [63].

From Fig. 17 it can also be noticed that the influence of water-binder ratio on the autogenous shrinkage of Portland cement paste is remarkable. This result is in line with the finding of other researchers [26,67,118]. With the increase of water-binder ratio, more free water is available in the pore structure of cement paste during the first seven days of hydration. More free water in the pore leads to higher internal

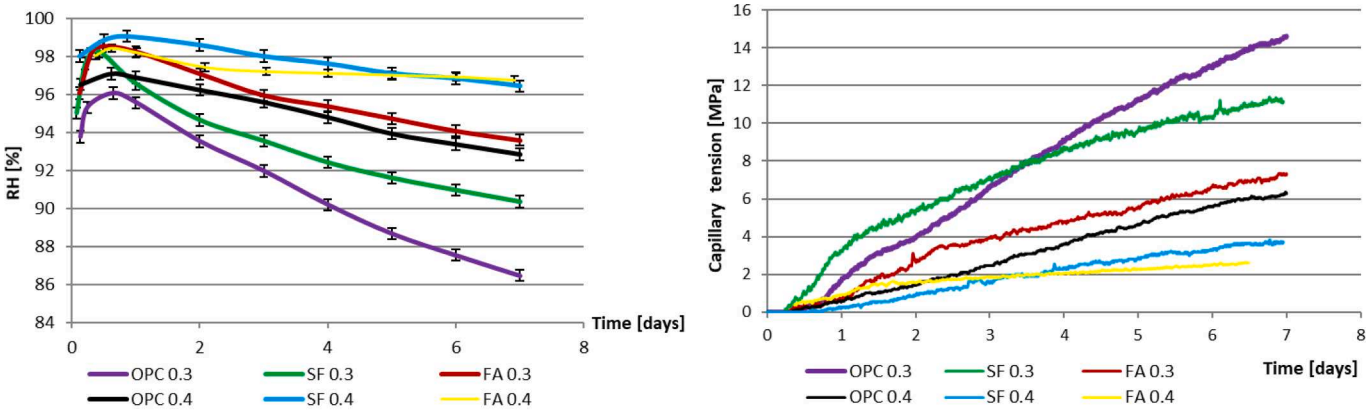

(a) Measured relative humidity (b) Capillary tension calculated with Eq. 16

Fig. 15. Measured relative humidity and Calculated capillary tension of different kinds of cement paste. (a) Measured relative humidity; (b) Capillary tension calculated with Eq. (16).

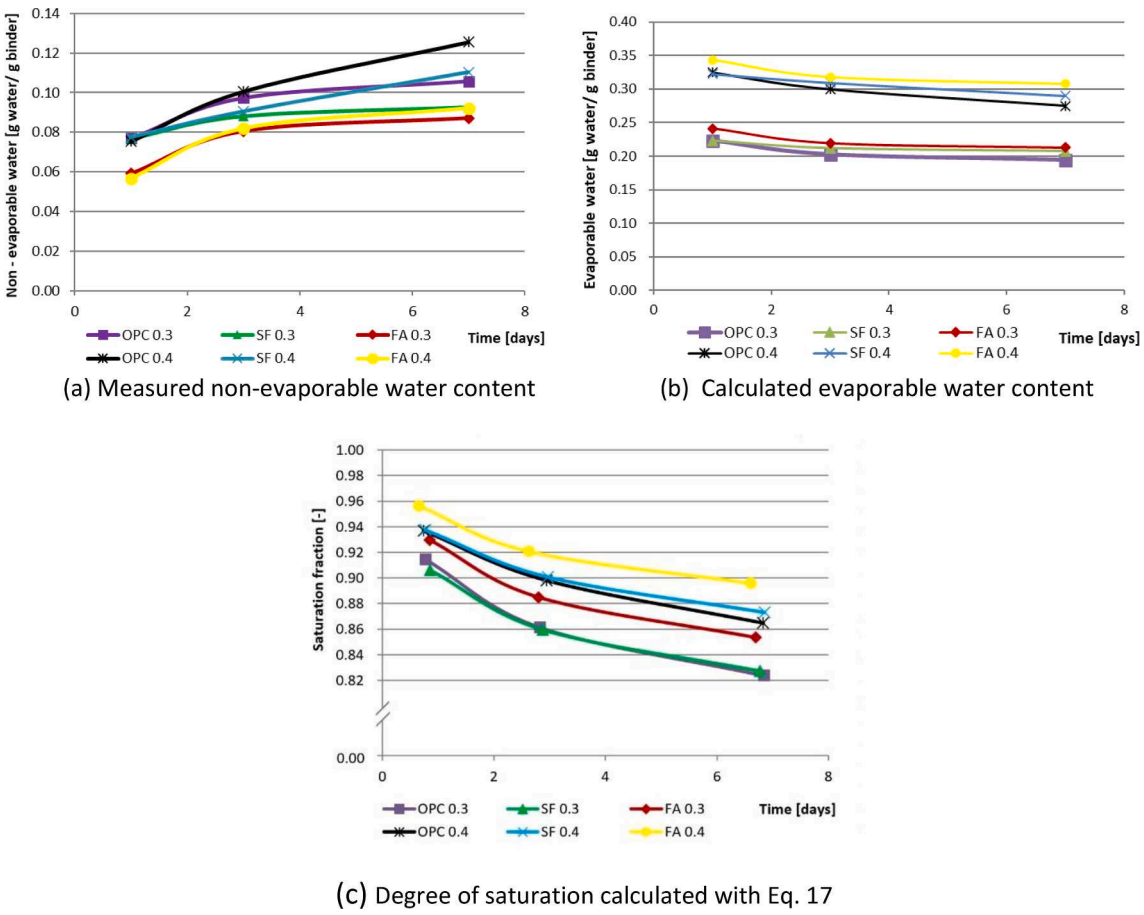

Fig. 16. Measured non-evaporable water content, calculated evaporable water content and degree of saturation of different kinds of cement paste specimens.

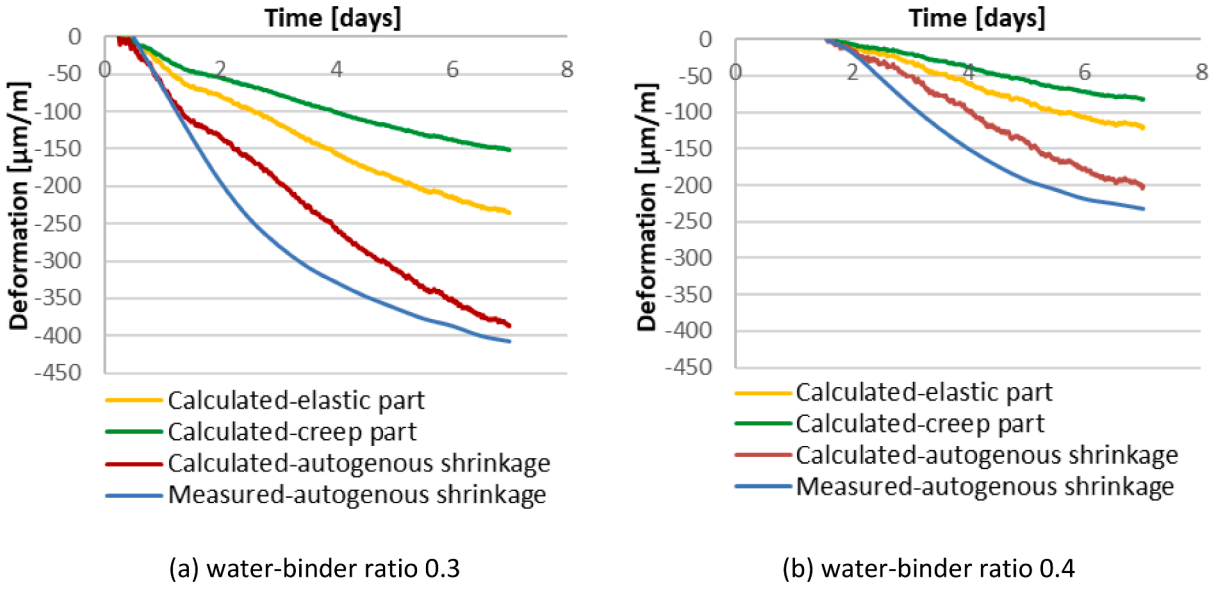

Fig. 17. Measured and calculated autogenous deformation of OPC paste with water-binder ratio of 0.3 and 0.4 after the maximum swelling (Time 0 day is the final setting time).

relative humidity (as shown in Fig. 8) and smaller driving force, i.e., capillary tension as shown in Fig. 15(b), of autogenous shrinkage. Although the increase of water binder ratio also decreases the stiffness of cement paste, e.g., elastic modulus (as shown in Fig. 14(b)), and resistance to deformation. The influence of the increasing water content on the driving force is more prominent and lead to smaller measured and calculated shrinkage.

5.4.2. Silica fume cement paste with water-binder ratio of 0.3 and 0.4

In Fig. 18(a and b), autogenous shrinkages of silica fume Portland

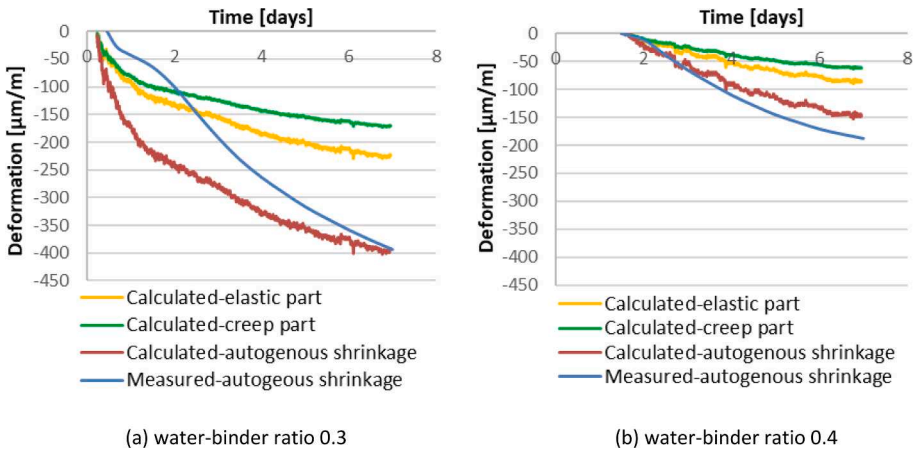

Fig. 18. Measured and calculated autogenous deformation of silica fume cement paste with water-binder ratio of 0.3 and 0.4 after the maximum swelling (Time 0 day is the final setting time).

cement pastes with 30% water-binder ratio 0.3 and 0.4 are presented. From Fig. 18(a) it can be noticed that the calculated autogenous shrinkage is bigger than the measured result at the first several days. This can be explained by the neglection of influence of the early age expansion in the proposed model. During the hydration process, the reaction can accompany with an external expansion which is supposed to be caused by several mechanisms e.g., crystal pressure and hydration dispersion [119,120]. The measured early-age deformation on macro-scale of cement paste is the result of the competition between expansion and shrinkage process as shown in Fig. 12. After the maximum swelling, the shrinkage process is dominant and the external volume of cement paste decreases. However, the expansion mechanism still plays a role in the deformation and the neglection of its influence will lead to the overestimation of autogenous shrinkage.

As shown in Figs. 8 and 15(b), the drop of relative humidity and increase of capillary tension of silica fume cement paste are smaller than these of Portland cement paste with same water-binder ratio. But from the comparison between Fig. 17 and Fig. 18, it can be noticed that the difference between the autogenous deformations of Portland cement paste and silica fume cement paste with same water-binder ratio is not pronounced. This is due to the fact that the stiffness of silica fume cement paste, i.e., compressive strength and elastic modulus as shown in Fig. 14, is lower than that of Portland cement paste. As discussed in Section 2, both capillary tension and mechanical properties together determine the magnitude of autogenous shrinkage. Lower stiffness leads to bigger autogenous shrinkage of silica fume cement paste with the similar capillary tension. Therefore, although the capillary tension of silica fume cement paste is smaller than that of Portland cement paste, the autogenous shrinkage of silica fume cement paste is similar to that of Portland cement paste.

5.4.3. *Fly ash cement paste with water-binder ratio of 0.3 and 0.4*

The calculated autogenous shrinkages of fly ash cement pastes with water-binder ratio 0.3 and 0.4 are shown in Fig. 19. From the comparison between Fig. 17 and Fig. 19, it can be noticed that the autogenous shrinkage of fly ash cement paste is significantly smaller than that of Portland cement paste with same water-binder ratio. Similar results can be found in other researchers' work [29–31]. For fly ash cement paste, the dosage of low active fly ash leads to higher effective water-binder ratio. As discussed in Section 5.4.1, the autogenous shrinkage of cement paste with higher water-binder ratio is smaller.

Fig. 19(a) shows that there is still some discrepancy between the measured and calculated results even the trend of the autogenous shrinkage is predicted quite well by using the proposed model. Besides early age expansion discussed in last section, the different ratio between the creep and elastic deformation of fly ash cement paste may be another reason of the discrepancy. According to Hu [83], the ratio between the creep and elastic deformation of fly ash cement paste is different with that of Portland cement paste and this can be attributed to the higher porosity of fly ash cement paste at early age. This influencing factor is not explicitly in the proposed model which may also leads to mis-estimating of autogenous shrinkage.

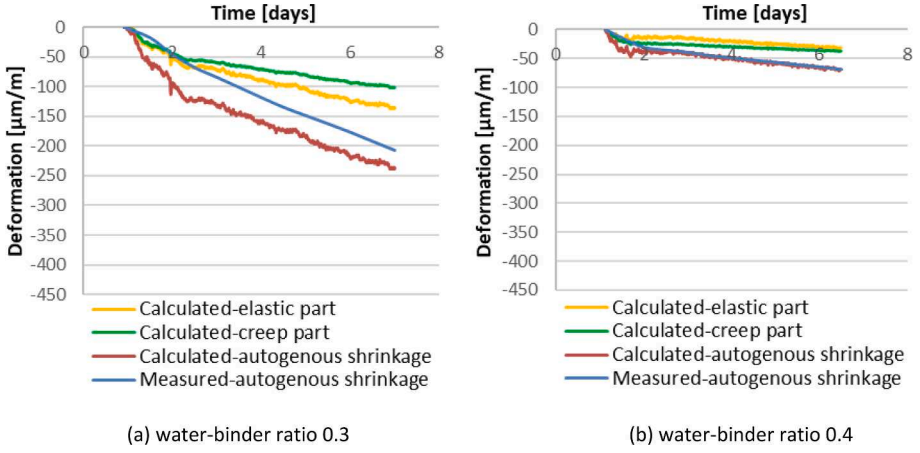

Fig. 19. Measured and calculated autogenous deformation of fly ash cement paste with water-binder ratio of 0.3 and 0.4 after the maximum swelling (Time 0 day is the final setting time).

5.5. Discussion

From Figs. 17-19 it can be found that the significance of creep part on the autogenous shrinkage is quite pronounced. By taking the creep into consideration the trend of autogenous shrinkage of different kinds of cement paste can be predicted quite well with the proposed model. But there are still some differences between the measured and calculated results as shown in Table 5. It should be realised that not all the factors of autogenous shrinkage are taken into consideration in the proposed model. The internal driving force and mechanical properties are the only considered influencing factors of autogenous shrinkage in the proposed model. The internal driving force and mechanical properties of cement paste with SCMs is calculated and then the autogenous shrinkage is predicted based on these calculated results. But the addition of SCMs will also affect other factors of autogenous deformation. For example, the proposed model does not take early age expansion into consideration which leads to discrepancy between the measured and calculated results during the first several days. The influences of different SCMs on the early age expansion are different and the magnitudes of the discrepancy of corresponding cement paste are different. Beside early age expansion, ion concentration of pore solution also influences capillary tension and autogenous shrinkage. According to Equation (15), the value of calculated capillary tension is affected by dissolved ions and measured relative humidity. The effect of dissolved ions in the pore solution on the calculated capillary tension changes with the ion concentration. In this study, the change of effect of dissolved ions is ignored. In fact, the ion concentration of pore water of cement paste increases with time during the first 28 days after mixing [3]. Its influence on the calculated capillary tension also increases with time. Without taking the increasing ion concentration of pore water into consideration may lead to misestimating of autogenous shrinkage. Other influencing factors of autogenous deformation which are re not taken into consideration in this study includes ratio between creep and elastic deformation, microcracking and relaxation [121–123]. In order to better predict autogenous shrinkage, further improvements of the proposed model by taking these effects into consideration are needed in the researchers' future work.

6. Conclusions

In this paper, the effect of SCMs, which include silica fume and fly ash, on physical properties and autogenous shrinkage of cement paste were experimentally studied. Based on the experiment results, it can be found that the addition of fly ash will significantly affect the physical properties. The relative final setting is prolonged and the non-evaporable water content decreases. The use of fly ash has negative influence on the compressive strength. The chemical and autogenous shrinkage of fly ash cement is smaller than that of Portland cement paste with same water-binder ratio. Low early-age reaction activity of fly ash is main reason of these measured results. The silica fume used in this paper is the dry densified silica fume. It is primarily in the form of linked clusters of particles. Its particle size is not much smaller than that of Portland cement. The reaction activity and filling effect of dry densified silica fume is not very noteworthy as silica fume in slurry form. The effect of dry densified silica fume on the physical properties and autogenous shrinkage is not very pronounced.

Autogenous shrinkage of Portland, silica fume and fly ash cement paste with water-binder ratios of 0.3 and 0.4 were also measured. The measured results show that autogenous shrinkages of cement pastes reduce significantly with the increase of water-binder ratio. The addition of fly ash will lead to smaller autogenous shrinkage while the influence of the dry densified silica fume on the autogenous shrinkage is not pronounced. A simulation model was proposed to predict the autogenous shrinkage of these different kinds of cement paste. In this model, the autogenous shrinkage is divided into an elastic part and a creep part, which are calculated separately. The creep part of this model is based on the solidification theory and takes the continuously changing physical properties of hardening cement paste into consideration. From the comparison between the calculated and measured results, it was found that the trend of autogenous shrinkage of different cement pastes can be predicted by using the proposed model quite well. However, several influencing factors of autogenous deformation are not taken into consideration in this model, e.g., early age expansion, ion concentration, ratio between creep and elastic deformation, micro-cracking and relaxation. Therefore, further improvements of the proposed model by taking these effects into consideration are needed for better prediction of autogenous shrinkage.

Table 5
Measured and calculated autogenous shrinkage of different kinds of cement pastes (Starting time: after the maximum swelling).

Name	Measured shrinkage at 7 days (μstrain)	Calculated shrinkage at 7 days (μstrain)	Deviation (|μ strain|)	Deviation (%)
OPC 0.3	407	386	21	5.16
SF 0.3	393	394	1	0.25
FA 0.3	205	238	33	16.10
OPC 0.4	232	205	27	11.64
SF 0.4	176	149	27	15.34
FA 0.4	75	76	1	1.33

CRediT authorship contribution statement

Tianshi Lu: Conceptualization, Methodology, Investigation, Software, Writing – original draft. **Jie Ren:** Writing – review & editing. **Xisheng Deng:** Investigation. **Zhenming Li:** Conceptualization, Methodology, Investigation, Writing – review & editing.

Declaration of Competing Interest

The authors declare that they have no known competing financial interests or personal relationships that could have appeared to influence the work reported in this paper.

Data availability

Data will be made available on request.

Acknowledgments

This research was supported by the National Natural Science Foundation of China (Grant Nos. 42271146). Horizon Europe guarantee funding (grant number EP/X022587/1) is acknowledged for the support of Zhenming Li.

References

[1] J.G. Olivier, K.M. Schure, J.A.H.W. Peters, Trends in global CO2 and total greenhouse gas emissions, PBL Netherlands Environmental Assessment Agency 5 (2017).
[2] L.J. Hanle, K.R. Jayaraman, J.S. Smith, CO2 emissions profile of the US cement industry, Environmental Protection Agency, Washington DC, 2004.
[3] H.F. Taylor, Cement chemistry 2 (1997) 459.
[4] R.P. Khatri, V. Sirivivatnanon, W. Gross, Effect of different supplementary cementitious materials on mechanical properties of high performance concrete, Cement and Concrete research 25 (1) (1995) 209–220.
[5] H. Toutanji, N. Delatte, S. Aggoun, R. Duval, A. Danson, Effect of supplementary cementitious materials on the compressive strength and durability of short-term cured concrete, Cement and concrete research 34 (2) (2004) 311–319.
[6] Safiuddin, M., & Zain, M. F. M. (2006). Supplementary cementing materials for high performance concrete.
[7] M.M. Johari, J.J. Brooks, S. Kabir, P. Rivard, Influence of supplementary cementitious materials on engineering properties of high strength concrete, Construction and Building Materials 25 (5) (2011) 2639–2648.

[8] K. Hanna, G. Morcous, M.K. Tadros, Effect of supplementary cementitious materials on the performance of concrete pavement, Journal of materials in civil engineering 26 (4) (2014) 789–793.
[9] A. Elahi, P.A.M. Basheer, S.V. Nanukuttan, Q.U.Z. Khan, Mechanical and durability properties of high performance concretes containing supplementary cementitious materials, Construction and Building Materials 24 (3) (2010) 292–299.
[10] A. Joshaghani, M.A. Moeini, M. Balapour, A. Moazenian, Effects of supplementary cementitious materials on mechanical and durability properties of high-performance non-shrinking grout (HPNSG), Journal of Sustainable Cement-Based Materials 7 (1) (2018) 38–56.
[11] J.B.A. Gedam, N.M. Bhandari, A. Upadhyay, Influence of supplementary cementitious materials on shrinkage, creep, and durability of high-performance concrete, Journal of Materials in Civil Engineering 28 (4) (2016) 04015173.
[12] A. Neville, P.C. Aitcin, High performance concrete—An overview, Materials and structures 31 (2) (1998) 111–117.
[13] M. Shafieifar, M. Farzad, A. Azizinamini, Experimental and numerical study on mechanical properties of Ultra High Performance Concrete (UHPC), Construction and Building Materials 156 (2017) 402–411.
[14] H.J. Chen, Y.L. Yu, C.W. Tang, Mechanical properties of ultra-high performance concrete before and after exposure to high temperatures, Materials 13 (3) (2020) 770.
[15] B. Persson, D.P. Bentz, G. Fagerlund, Self-desiccation and its importance in concrete technology: Proceedings of the fourth international research seminar, Gaithersburg, Maryland, USA, June 2005, Division of Building Materials, LTH, Lund University, 2005.
[16] E. Tazawa, Autogenous shrinkage of concrete, E&F SPON, London and New York, 1998.
[17] D.P. Bentz, W.J. Weiss, Internal Curing: a 2010 State-of-the-Art Review, NISTIR 7765, U.S. Department of Commerce, 2011.
[18] F. Liu, J. Wang, X. Qian, J. Hollingsworth, Internal curing of high performance concrete using cenospheres, Cement and Concrete Research 95 (2017) 39–46.
[19] T. Lu, Autogenous Deformation of Early Age Cement Paste and Mortar, Technische Universiteit Delft, Delft, The Netherlands, 2019. Ph.D. Thesis.
[20] Y. Akkaya, C. Ouyang, S.P. Shah, Effect of supplementary cementitious materials on shrinkage and crack development in concrete, Cement and Concrete Composites 29 (2) (2007) 117–123.
[21] Y. Li, Q.Q. Yan, Relationship between Internal Relative Humidity and Autogenous Shrinkage of Cement Paste with Supplementary Cementitious Materials (SCM), in: Key Engineering Materials, Vol. 539, Trans Tech Publications Ltd., 2013, pp. 35–39.
[22] E. Ghafari, S.A. Ghahari, H. Costa, E. Júlio, A. Portugal, L. Durães, Effect of supplementary cementitious materials on autogenous shrinkage of ultra-high performance concrete, Construction and Building Materials 127 (2016) 43–48.
[23] T. Lu, Z. Li, H. Huang, Effect of supplementary materials on the autogenous shrinkage of cement paste, Materials 13 (15) (2020) 3367.
[24] S.I. Igarashi, A. Bentur, K. Kovler, Autogenous shrinkage and induced restraining stresses in high-strength concretes, Cement and Concrete Research 30 (11) (2000) 1701–1707.
[25] K.M. Lee, H.K. Lee, S.H. Lee, G.Y. Kim, Autogenous shrinkage of concrete containing granulated blast-furnace slag, Cement and Concrete Research 36 (7) (2006) 1279–1285.
[26] M.H. Zhang, C.T. Tam, M.P. Leow, Effect of water-to-cementitious materials ratio and silica fume on the autogenous shrinkage of concrete, Cement and Concrete Research 33 (10) (2003) 1687–1694.
[27] L. Wu, N. Farzadnia, C. Shi, Z. Zhang, H. Wang, Autogenous shrinkage of high performance concrete: A review, Construction and Building Materials 149 (2017) 62–75.
[28] G. Hong, S. Choi, Effect of dispersibility of carbon nanotubes by silica fume on material properties of cement mortars: Hydration, pore structure, mechanical properties, self-desiccation, and autogenous shrinkage, Construction and Building Materials 265 (2020), 120318.
[29] H.K. Lee, K.M. Lee, B.G. Kim, Autogenous shrinkage of high-performance concrete containing fly ash, Magazine of concrete research 55 (6) (2003) 507–515.
[30] S.W. Yoo, S.J. Kwon, S.H. Jung, Analysis technique for autogenous shrinkage in high performance concrete with mineral and chemical admixtures, Construction and Building Materials 34 (2012) 1–10.
[31] Y. Gao, H. Zhang, S. Tang, H. Liu, Study on early autogenous shrinkage and crack resistance of fly ash high-strength lightweight aggregate concrete, Magazine of concrete research 65 (15) (2013) 906–913.
[32] O.M. Jensen, P.F. Hansen, Autogenous relative humidity change in silica fume-modified cement paste, Advances in Cement Research 7 (25) (1995) 33–38.
[33] M. Jensen, P.F. Hansen, Autogenous deformation and change of the relative humidity in silica fume-modified cement paste, Materials Journal 93 (6) (1996) 539–543.
[34] I. De la Varga, J. Castro, D. Bentz, J. Weiss, Application of internal curing for mixtures containing high volumes of fly ash, Cement and Concrete Composites 34 (9) (2012) 1001–1008.
[35] P. Lura, Autogenous deformation and internal curing of concrete, Delft University of Technology, 2003. PhD thesis.
[36] R. Sharma, R.A. Khan, Effect of different supplementary cementitious materials on mechanical and durability properties of concrete, Journal of Materials and Engineering Structures «JMES» 3 (3) (2016) 129–147.
[37] M. Mazloom, A.A. Ramezanianpour, J.J. Brooks, Effect of silica fume on mechanical properties of high-strength concrete, Cement and Concrete Composites 26 (4) (2004) 347–357.
[38] A.A. Ramezanianpour, V.M. Malhotra, Effect of curing on the compressive strength, resistance to chloride-ion penetration and porosity of concretes incorporating slag, fly ash or silica fume, Cement and concrete composites 17 (2) (1995) 125–133.
[39] P. Chindaprasirt, C. Jaturapitakkul, T. Sinsiri, Effect of fly ash fineness on compressive strength and pore size of blended cement paste, Cement and concrete composites 27 (4) (2005) 425–428.
[40] K. Trill, M. Kawamura, Pore structure and chloride permeability of concretes containing fly ash, blast furnace slag and silica fume, Special Publication 132 (1992) 135–150.
[41] L. Bagel, Strength and pore structure of ternary blended cement mortars containing blast furnace slag and silica fume, Cement and Concrete Research 28 (7) (1998) 1011–1022.
[42] Z. Yu, G. Ye, The pore structure of cement paste blended with fly ash, Construction and Building Materials 45 (2013) 30–35.
[43] M. Oltulu, R. Şahin, Pore structure analysis of hardened cement mortars containing silica fume and different nano-powders, Construction and Building Materials 53 (2014) 658–664.
[44] Q. Zeng, K. Li, T. Fen-Chong, P. Dangla, Pore structure characterization of cement pastes blended with high-volume fly-ash, Cement and Concrete Research 42 (1) (2012) 194–204.
[45] R. Defay, I. Prigogine, A. Bellemans, Surface tension and adsorption, Wiley, 1966.
[46] B. Persson, Correlating laboratory and field tests of creep in high-performance concrete, Cement and concrete Research 31 (3) (2001) 389–395.
[47] Van Breugel, K. (1993). Simulation of hydration and formation of structure in hardening cement-based materials.
[48] P.K. Mehta, P.J. Monteiro, Concrete: microstructure, properties, and materials, McGraw-Hill Education, 2014.
[49] P. Klug, F. Wittmann, Activation energy of creep of hardened cement paste, Matériaux et Construction 2 (1) (1969) 11–16.
[50] Z.P. Bažant, E. Osman, Double power law for basic creep of concrete, Matériaux et Construction 9 (1) (1976) 3–11.
[51] Z.P. Bažant, J.C. Chern, Triple power law for concrete creep, Journal of Engineering Mechanics 111 (1) (1985) 63–83.
[52] Z.P. Bazant, W.P. Murphy, Creep and shrinkage prediction model for analysis and design of concrete structures-model B3, Matériaux et constructions 28 (180) (1995) 357–365.
[53] A. Hilaire, F. Benboudjema, A. Darquennes, Y. Berthaud, G. Nahas, Modeling basic creep in concrete at early-age under compressive and tensile loading, Nuclear Engineering and Design 269 (2014) 222–230.
[54] C.h. Pichler, R. Lackner, A multiscale creep model as basis for simulation of early-age concrete behavior, Computers and Concrete 5 (4) (2008) 295–328.
[55] B.D. Hedegaard, Multi-Decade, Multi-Scale Modeling of Aging Basic Creep of Concrete, ACI Materials Journal 117 (6) (2020) 17–27.
[56] M. Rasoolinejad, S. Rahimi-Aghdam, Z.P. Bažant, Prediction of autogenous shrinkage in concrete from material composition or strength calibrated by a large database, as update to model B4, Materials and Structures 52 (2) (2019) 1–17.
[57] Z. Bažant, M. Hubler, R. Wendner, Model B4 for creep, drying shrinkage and autogenous shrinkage of normal and high-strength concretes with multi-decade applicability, RILEM Technical Committee TC-242-MDC (2015) 9.
[58] F.I. Du Béton, Model code 2010: final draft, International Federation for Structural Concrete, 2012.
[59] G.C. Fanourakis, Validation of the FIB 2010 and RILEM B4 models for predicting creep in concrete, Architecture Civil Engineering Environment 95 (2017) 95–101.
[60] Fanourakis, G. C. (2017). Evaluation of the creep coefficients of the FIB 2010 and RILEM B4 concrete creep prediction models. In 12th Central European Congress on Concrete Engineering.
[61] C. Hua, P. Acker, A. Ehrlacher, Analyses and models of the autogenous shrinkage of hardening cement paste: I. Modelling at macroscopic scale, Cement and Concrete research 25 (7) (1995) 1457–1468.
[62] M. Wyrzykowski, P. Lura, F. Pesavento, D. Gawin, Modeling of internal curing in maturing mortar, Cement and Concrete Research 41 (12) (2011) 1349–1356.
[63] Z. Hu, M. Wyrzykowski, K. Scrivener, P. Lura, Prediction of autogenous shrinkage of cement pastes as poro-visco-elastic deformation, Cement and Concrete Research 126 (2019) 105917.
[64] T. Lu, Z. Li, H. Huang, Restraining effect of aggregates on autogenous shrinkage in cement mortar and concrete, Construction and Building Materials 289 (2021) 123166.
[65] Z.P. Bazant, S. Prasannan, Solidification theory for concrete creep, I: Formulation. Journal of engineering mechanics 115 (8) (1989) 1691–1703.
[66] Z.P. Bažant, S. Prasannan, Solidification theory for concrete creep. II: Verification and application, Journal of Engineering mechanics 115 (8) (1989) 1704–1725.
[67] E.I. Tazawa, S. Miyazawa, Experimental study on mechanism of autogenous shrinkage of concrete, Cement and Concrete Research 25 (8) (1995) 1633–1638.
[68] S. Hanehara, H. Hirao, H. Uchikawa, Relationships between autogenous shrinkage and the microstructure and humidity changes at inner part of hardened cement paste at early age, Autogenous Shrinkage of Concrete, E&FN Spon, London (1999) 93–104.
[69] P. Lura, O.M. Jensen, K. Van Breugel, Autogenous shrinkage in high-performance cement paste: An evaluation of basic mechanisms, Cement and concrete research 33 (2) (2003) 223–232.

[70] W.G. Gray, B.A. Schrefler, Thermodynamic approach to effective stress in partially saturated porous media, European Journal of Mechanics-A/Solids 20 (4) (2001) 521–538.
[71] D. Gawin, F. Pesavento, B.A. Schrefler, Modelling creep and shrinkage of concrete by means of effective stresses, Materials and Structures 40 (6) (2007) 579–591.
[72] O.M. Jensen, Thermodynamic limitation of self-desiccation, Cement and Concrete Research 25 (1) (1995) 157–164.
[73] M.J. Setzer, ,The Munich Model-An Example for Modern Materials Science in, in: Civil Engineering, In: Gerdes, A.: Advances in Building Materials Science-Research and Applications, AEDIFICATIO Publishers, Freiburg and Unterengstringen, 1996, p. 3.
[74] C. Di Bella, M. Wyrzykowski, P. Lura, Evaluation of the ultimate drying shrinkage of cement-based mortars with poroelastic models, Materials and Structures 50 (1) (2017) 1–13.
[75] B. Hedegaard, Creep and Shrinkage Modeling of Concrete Using Solidification Theory, Journal of Materials in Civil Engineering 32 (7) (2020) 04020179.
[76] Neville, A. M. (1983). Creep of plain and structural concrete.
[77] R. Mabrouk, T. Ishida, K. Maekawa, A unified solidification model of hardening concrete composite for predicting the young age behavior of concrete, Cement and Concrete Composites 26 (5) (2004) 453–461.
[78] S.Y. Abate, S. Park, H.-K. Kim, Parametric modeling of autogenous shrinkage of sodium silicate-activated slag, Construction and Building Materials 262 (2020) 120747.
[79] Z.P. Bažant, S.S. Kim, Nonlinear creep of concrete—adaptation and flow, Journal of the Engineering Mechanics Division 105 (3) (1979) 429–446.
[80] Y. Lee, S.T. Yi, M.S. Kim, J.K. Kim, Evaluation of a basic creep model with respect to autogenous shrinkage, Cement and concrete research 36 (7) (2006) 1268–1278.
[81] M.H. Hubler, R. Wendner, Z.P. Bažant, Comprehensive Database for Concrete Creep and Shrinkage: Analysis and Recommendations for Testing and Recording, ACI Materials Journal 112 (4) (2015).
[82] O. Coussy, P. Dangla, T. Lassabatère, V. Baroghel-Bouny, The equivalent pore pressure and the swelling and shrinkage of cement-based materials, Materials and structures 37 (1) (2004) 15–20.
[83] Hu, Z. (2017). Prediction of autogenous shrinkage in fly ash blended cement systems (No. THESIS). EPFL.
[84] S. Diamond, S. Sahu, Densified silica fume: particle sizes and dispersion in concrete, Materials and Structures 39 (9) (2006) 849–859.
[85] ASTM, C. (1999). Standard practice for mechanical mixing of hydraulic cement pastes and mortars of plastic consistency. In American Society for Testing and Materials. 305-99.
[86] EN, D. (2009). Methods of testing cement—part 3: determination of setting times and soundness.
[87] Z. Li, S. Zhang, Y. Zuo, et al., Chemical deformation of metakaolin based geopolymer[J], Cement and Concrete Research 120 (2019) 108–118.
[88] Astm, a., C1698–09 Standard test method for autogenous strain of cement paste and mortar, ASTM International, West Conshohocken, PA, 2009.
[89] O.M. Jensen, P.F. Hansen, A dilatometer for measuring autogenous deformation in hardening Portland cement paste, Materials and structures 28 (7) (1995) 406–409.
[90] K. Marar, Effect of cement content and water/cement ratio on fresh concrete properties without admixtures, International Journal of Physical Sciences 6 (24) (2011) 5752–5765.
[91] J. Hu, Z. Ge, K. Wang, Influence of cement fineness and water-to-cement ratio on mortar early-age heat of hydration and set times, Construction and building materials 50 (2014) 657–663.
[92] N. Dave, A.K. Misra, A. Srivastava, S.K. Kaushik, Setting time and standard consistency of quaternary binders: The influence of cementitious material addition and mixing, International Journal of Sustainable Built Environment 6 (1) (2017) 30–36.
[93] Zhutovsky, S., & Kovler, K. (2009). Effect of water to cement ratio and degree of hydration on chemical shrinkage of cement pastes. In 2nd International RILEM Workshop on Concrete Durability and Service Life Planning, ConcreteLife'09 (pp. 47-54).
[94] X. Pang, D.P. Bentz, C. Meyer, G.P. Funkhouser, R. Darbe, A comparison study of Portland cement hydration kinetics as measured by chemical shrinkage and isothermal calorimetry, Cement and Concrete Composites 39 (2013) 23–32.
[95] Fang, Y. H., Gu, Y. M., & Kang, Q. B. (2011). Effect of fly ash, MgO and curing solution on the chemical shrinkage of alkali-activated slag cement. In Advanced Materials Research (Vol. 168, pp. 2008-2012). Trans Tech Publications Ltd.
[96] V. Yogendran, B.W. Langan, M.A. Ward, Hydration of cement and silica fume paste, Cement and Concrete Research 21 (5) (1991) 691–708.
[97] M.H. Zhang, O.E. Gjørv, Effect of silica fume on cement hydration in low porosity cement pastes, Cement and Concrete Research 21 (5) (1991) 800–808.
[98] Y. Maltais, J. Marchand, Influence of curing temperature on cement hydration and mechanical strength development of fly ash mortars, Cement and concrete research 27 (7) (1997) 1009–1020.
[99] N. Schwarz, N. Neithalath, Influence of a fine glass powder on cement hydration: Comparison to fly ash and modeling the degree of hydration, Cement and Concrete Research 38 (4) (2008) 429–436.
[100] S. Popovics, J. Ujhelyi, Contribution to the concrete strength versus water-cement ratio relationship, Journal of Materials in Civil Engineering 20 (7) (2008) 459–463.
[101] O. Alawode, O.I. Idowu, Effects of water-cement ratios on the compressive strength and workability of concrete and lateritic concrete mixes, The Pacific Journal of Science and Technology 12 (2) (2011) 99–105.
[102] S.B. Singh, P. Munjal, N. Thammishetti, Role of water/cement ratio on strength development of cement mortar, Journal of Building Engineering 4 (2015) 94–100.
[103] H.A. Toutanji, T. El-Korchi, The influence of silica fume on the compressive strength of cement paste and mortar, Cement and Concrete Research 25 (7) (1995) 1591–1602.
[104] M. Chang-Wen, T. Qian, S. Wei, L. Jia-Ping, Water consumption of the early-age paste and the determination of "time-zero" of self-desiccation shrinkage, Cement and concrete research 37 (11) (2007) 1496–1501.
[105] Bentur A., 2002. Terminology and definitions, in: K. Kovler, A. Bentur (Eds.). International RILEM Conference on Early Age Cracking in Cementitious Systems—EAC, RILEM TC181-EAS, Haifa 2002, pp. 13–20.
[106] A. Darquennes, S. Staquet, M.P. Delplancke-Ogletree, B. Espion, Effect of autogenous deformation on the cracking risk of slag cement concretes, Cement and Concrete Composites 33 (3) (2011) 368–379.
[107] G. Sant, F. Rajabipour, P. Lura, J. Weiss, Examining time-zero and early age expansion in pastes containing shrinkage reducing admixtures (SRA's). In Proc., 2nd RILEM Symp. on Advances in Concrete through Science and Engineering, 2006.
[108] Weiss J., 2003. Experimental Determination of the 'Time Zero' to (Maturity-Zero Mo), RILEM Report 25, Early Age Cracking in Cementitious Systems, Edited by A. Bentur, RILEM Publications S.A.R.L., Cachan, France, pp. 195-206.
[109] K. Kovler, D. Cusson, Effects of internal curing on autogenous deformation, Internal Curing of Concrete-State-of-the-Art Report of RILEM Technical Committee 196-ICC (2007) 71–104.
[110] Z. Li, T. Lu, X. Liang, et al., Mechanisms of autogenous shrinkage of alkali-activated slag and fly ash pastes[J], Cement and Concrete Research 135 (2020), 106107.
[111] Ø. Bjøntegaard, Thermal dilatation and autogenous deformation as driving forces to self-induced stresses in high performance concrete, Norwegian University of Science and Technology, Norway, 1999. Ph.D. Thesis.
[112] F.A. Oluokun, E.G. Burdette, J.H. Deatherage, Elastic modulus, Poisson's ratio, and compressive strength relationships at early ages, Materials Journal 88 (1) (1991) 3–10.
[113] T. Noguchi, F. Tomosawa, K.M. Nemati, B.M. Chiaia, A.P. Fantilli, A practical equation for elastic modulus of concrete, ACI Structural Journal 106 (5) (2009) 690.
[114] H.J. Butt, M. Kappl, Normal capillary forces, Advances in colloid and interface science 146 (1–2) (2009) 48–60.
[115] C.L. Page, Ø. Vennesland, Pore solution composition and chloride binding capacity of silica-fume cement pastes, Matériaux et construction 16 (1) (1983) 19–25.
[116] P. Mazur, Kinetics of water loss from cells at subzero temperatures and the likelihood of intracellular freezing, The Journal of general physiology 47 (2) (1963) 347–369.
[117] T.C. Powers, T.L. Brownyard, September). Studies of the physical properties of hardened Portland cement paste, In Journal Proceedings (Vol. 43 (9) (1946) 101–132.
[118] Z. Jiang, Z. Sun, P. Wang, Autogenous relative humidity change and autogenous shrinkage of high-performance cement pastes, Cement and Concrete Research 35 (8) (2005) 1539–1545.
[119] E.M. Winkler, P.C. Singer, Crystallization pressure of salts in stone and concrete, Geological society of America bulletin 83 (11) (1972) 3509–3514.
[120] Budnikov, P. P., & Strelkov, M. I. (1966). Some recent concepts on Portland cement hydration and hardening. Highway Research Board Special Report, (90).
[121] Z. Li, T. Lu, Y. Chen, et al., Prediction of the autogenous shrinkage and microcracking of alkali-activated slag and fly ash concrete[J], Cement and Concrete Composites 117 (2021), 103913.
[122] S. Igarashi, A. Bentur, K. Kovler, Stresses and creep relaxation induced in restrained autogenous shrinkage of high-strength pastes and concretes, Advances in Cement Research 11 (4) (1999) 169–177.
[123] P. Lura, O.M. Jensen, J. Weiss, Cracking in cement paste induced by autogenous shrinkage, Materials and structures 42 (8) (2009) 1089–1099.